Pivotal roles of *Plasmodium falciparum* lysophospholipid acyltransferase 1 in cell cycle progression and cytostome internalization

Junpei Fukumoto[1,2*], Minako Yoshida[1,#], Suzumi M. Tokuoka[3,#], Eri Saki H. Hayakawa[4,#], Shinya Miyazaki[1], Takaya Sakura[5], Daniel Ken Inaoka[5,6], Kiyoshi Kita[6,7], Jiro Usukura[8], Hideo Shindou[9,10], Fuyuki Tokumasu[1,6*]

[1]Department of Cellular Architecture Studies, Division of Shionogi Global Infectious Diseases Division, Institute of Tropical Medicine (NEKKEN), Nagasaki 852-8523, Japan
[2]Research Fellow of Japan Society for the Promotion of Science
[3]Department of Lipidomics, Graduate School of Medicine, University of Tokyo, Tokyo 113-0033, Japan
[4]Division of Medical Zoology, Department of Infection and Immunity, Jichi Medical University, Tochigi 329-0498, Japan
[5]Department of Molecular Infection Dynamics, Division of Shionogi Global Infectious Diseases Division, Institute of Tropical Medicine (NEKKEN), Nagasaki 852-8523, Japan
[6]School of Tropical Medicine and Global Health, Nagasaki University, Nagasaki 852-8523, Japan
[7]Department of Host - Defense Biochemistry, Institute of Tropical Medicine (NEKKEN), Nagasaki University, Nagasaki 852−8523, Japan
[8]Institute of Materials and Systems for Sustainability, Nagoya University, Furo-cho, Nagoya 464-8601, Japan
[9]Department of Lipid Life Science, National Center for Global Health and Medicine, Shinjuku-ku, Tokyo 162-8655, Japan
[10]Department of Medical Lipid Science, Graduate School of Medicine, The University of Tokyo, Bunkyo-ku, Tokyo 113-8654, Japan

*Corresponding Authors: Fuyuki Tokumasu, Ph.D., Junpei Fukumoto, Ph.D.
Department of Cellular Architecture Studies,
Division of Shionogi Global Infectious Diseases,
Institute of Tropical Medicine (NEKKEN),
Nagasaki 852-8523, Japan
TEL: 095-819-7870
FAX: 095-819-7846
Email: ftokumasu@nagasaki-u.ac.jp
jfukumoto@nagasaki-u.ac.jp

#Equally contributing authors.

Running Title: PfLPLAT1 is essential for asexual cell division

Keywords: *Plasmodium falciparum*; malaria; lipid metabolism; lysophospholipid acyltransferase (LPLAT); cell cycle progression; conditional knockout

Abstract

The rapid intraerythrocytic replication of *Plasmodium falciparum*, a deadly species of malaria parasite, requires a quick but constant supply of phospholipids to support marked cell membrane expansion. In the malarial parasite, many enzymes functioning in phospholipid synthesis pathway have not been identified or characterized. Here, we identified *P. falciparum* lysophospholipid acyltransferase 1 (PfLPLAT1) and showed that PfLPLAT1 is vital for asexual parasite cell cycle progression and cytostome internalization. Deficiency in PfLPLAT1 resulted in decreased parasitemia and prevented transition to the schizont stage. Parasites lacking PfLPLAT1 also exhibited distinctive omega-shaped vacuoles, indicating disrupted cytostome function. Transcriptomic analyses suggested that this deficiency impacted DNA replication and cell cycle regulation. Mass spectrometry-based enzyme assay and lipidomic analysis demonstrated that recombinant PfLPLAT1 exhibited lysophospholipid acyltransferase activity with a preference for unsaturated fatty acids as its acyl donors and lysophosphatidic acids as an acceptor, with its conditional knockout leading to abnormal lipid composition and marked morphological and developmental changes including stage arrest. These findings highlight PfLPLAT1 as a potential target for antimalarial therapy, particularly due to its unique role and divergence from human orthologs.

59 **Introduction**

60 Malaria is a major mosquito-borne infectious disease that causes a large number of
61 deaths worldwide. During its intraerythrocytic stages, the parasite invades human
62 erythrocytes and encircles itself with a multi-layered membrane structure, which allows
63 communication with the external environment through the uptake of nutrients and the
64 expression of parasitic proteins on the surface of erythrocyte membranes. Both liver-
65 stage and erythrocytic-stage malaria parasites undergo rapid cell proliferation inside
66 the host cells, which requires a large amount of lipid molecules to support the
67 significant increase in the total cell surface area caused by the complex membrane
68 morphology[1]. Therefore, tight regulation of lipid levels and classes are important for
69 the normal proliferation of parasites.

70 In recent years, lipid metabolism and related areas in malaria parasites have been
71 drawing attention in the study of the roles of lipids in the complex regulation of
72 molecular pathways in parasites and as new drug targets[2]. These studies suggested
73 that parasites can acquire a wide variety of lipids from the erythrocyte cytoplasm and
74 extracellular environment, but they also synthesize them to meet stage-dependent
75 demands for specific lipid classes[3]. Lipid synthesis throughout the life cycle of malaria
76 parasites range from fatty acid synthesis to lipid droplet formation with neutral lipids[2,4].
77 Although most lipid classes can also be scavenged from the host cytoplasm and

78 extracellular environment, parasites must maintain a stable balance of fatty acids and
79 phospholipid and neutral lipid synthesis to meet the diverse needs of these molecules
80 at different stages and environments[5-8].

81 In mammalian cells, phospholipid *de novo* synthesis starts from the incorporation of
82 acyl-CoA into glycerol 3-phophate (G3P) by glycerol 3-phosphate acyltransferases
83 (GPATs) to produce lysophosphatidic acid (LPA). This reaction is followed by
84 additional acyl chain incorporation to produce phosphatidic acid (PA) and subsequent
85 head group modifications to produce diacylglycerol (DAG) and phospholipids
86 (Kennedy cycle)[9]. Acyl chains of these phospholipids are often excised by
87 phospholipases, and the resulting lysophospholipids (LPLs) can be processed back to
88 diacyl phospholipids with different combinations of acyl chains by lysophospholipid
89 acyltransferases (LPLATs) (Lands' cycle)[10]. To date, 14 mammalian LPLATs have
90 been identified from two independent families, 1-acylglycerol-3-phosphate O-
91 acyltransferase (AGPAT) and membrane-bound O-acyltransferase (MBOAT), based
92 on their primary structures (Table 1). These two families possess AGPAT[11,12] and
93 MBOAT motifs[13], respectively, which are essential for LPLAT activity. Each LPLAT
94 has multiple substrate specificities[14].The study of phospholipid heterogeneity created
95 by a series of acyltransferases and their relative expression levels in tissues has been

96 a rapidly growing area in the understanding of the complex regulation of this cell
97 biology, as well as in the search for unique disease markers.[15,16]
98 In contrast to the mammalian studies, data regarding the equivalent enzymes and
99 the uniqueness of phospholipid synthesis in *Plasmodium* spp. remain limited. Several
100 genes have been suggested as potential acyltransferases by the PlasmoDB database
101 (https://plasmodb.org/plasmo/app/), and only putative GPAT[17-19] and diacylglycerol
102 acyltransferase (DGAT)[20,21-22] have been examined for their activity and localization.
103 The ability of GPAT and DGAT to incorporate acyl chains into their substrates, G3P
104 and DAG, respectively, was estimated using whole-cell lysates or by heterogenous
105 expression in *Escherichia coli* (*E. coli*) or yeast, but the enzymatic activity of
106 recombinant parasite proteins was not investigated, probably because of the technical
107 complexity of assessing acyltransferase activity in vitro. Moreover, no studies have
108 been conducted to identify and characterize LPLATs in *P. falciparum*, although two
109 estimated LPLATs were researched in the liver stage of *Plasmodium yoelii*[18]. We
110 performed a database search with the mammalian AGPAT motif (Fig. 1B), which
111 contains four core functional domains[11,23,12], as a model sequence, and identified a
112 gene in *P. falciparum* that potentially has LPLAT activity: no genes were identified by
113 the MBOAT motif.

114 Here we report the identification and first systematic characterization of a *P.*
115 *falciparum* LPLAT, which we named PfLPLAT1. Liquid chromatography-tandem mass
116 spectrometry (LC-MS/MS) analysis showed that recombinant PfLPLAT1 incorporates
117 acyl chains into PA (lysophosphatidic acid acyl transferase, or LPAAT activity) and
118 lysophosphatidylcholine (LPC) (lysophosphatidylcholine acyltransferase, or LPCAT
119 activity), with a preference against PA as a substrate (acceptor) and unsaturated fatty
120 acids as acyl chain donors. Conditional knockout of this gene showed a marked growth
121 defect with a failure in stage transition. These phenotypes are also associated with a
122 characteristic cytostome structural abnormality, which is an essential membrane
123 invagination process for the uptake of host erythrocyte cytoplasm to acquire
124 hemoglobin and other nutrients. Our data suggest the importance of PA in cytostome
125 formation and cell cycle progression in malaria parasites.

126 **Results**

127 **Catalytic motifs of LPLATs are conserved in a wide variety of organisms**

128 **including *P. falciparum***

129 In the phospholipid biosynthesis pathway, LPLATs convert LPLs (mono-acyl form)

130 to PLs (di-acyl form) by incorporating an acyl chain into the glycerol back bone (Fig

131 1A). Mammalian LPLATs are members of either the AGPAT family or MBOAT family,

132 and some mammalian LPLAT isoforms have lysophosphatidylcholine acyltransferase

133 (LPCAT), lysophosphatidylethanolamine acyltransferase (LPEAT),

134 lysophosphatidylinositol aclytransferase (LPIAT), and LPAAT activity in the Lands

135 cycle[14]. Because of the flexible substrate specificity of LPLATs, it is more appropriate

136 to avoid specifying substrate preferences in their names, and simply sort them with

137 numbers[14].

138 To identify LPLATs in *P. falciparum*, we first performed a database search using

139 AGPAT motifs[11,12] of murine LPLAT8 as bait sequences and found an entry

140 designated as a putative *P. falciparum* LPLAT (ID: PF3D7_1444300, designated as 1-

141 acyl-*sn*-glycerol-3-phosphate acyltransferase or LPAAT). We named this protein as *P.*

142 *falciparum* lysophospholipid acyltransferase 1 PfLPLAT1, in accordance with

143 previously proposed nomenclature[14]. PfLPLAT1 is predicted to have two

144 transmembrane domains (amino acids 21–43 and 51–80) at the N-terminus and an

145 AGPAT domain (amino acids 94–220) at the C-terminus (Fig 1C). It has been revealed
146 that AGPAT motifs (motifs I–IV) are essential for LPLAT activity in mammalian
147 LPLATs[11,12]. We compared the amino acid sequences with those of putative LPLATs
148 from other organisms (Fig 1D). Multiple alignment showed that motif I (HxxxxD) and
149 motif III (xxEG(TR)) were conserved in *P. falciparum*, while motif II (GxxFxxR) had
150 lower sequence similarity. Motif IV (xxxxPxx) is characterized by a proline residue
151 surrounded by nonpolar amino acids. Although the proline is conserved in PfLPLAT1
152 motif IV, it is followed by cysteine, which is a polar residue. Considering motif IV is
153 generally less conserved among all AGPATs, it is questionable whether PfLPLAT1
154 motif IV is involved in the acyltransferase activity. Despite the low conservation of
155 amino acid residues in motif II and IV, prediction of its three-dimensional conformation
156 showed that spatial arrangements of motifs I–IV of PfLPLAT1 were similar to those of
157 *Homo sapiens* LPLAT1 (HsAGPAT1) [26] (Fig 1E).
158

159 **Recombinant PfLPLAT1 exhibits lysophospholipid acyltransferase activity**

160 Because the AGPAT motifs in PfLPLAT1 are not perfectly conserved, the enzymatic
161 activity of PfLPLAT1 as an acyltransferase must be examined. To confirm whether
162 PfLPLAT1 is an LPLAT, we tested its enzymatic activity by LC-MS/MS analysis, with
163 recombinant PfLPLAT1 synthesized by a wheat germ expression system (Fig 2A). We

164 expressed PfLPLAT1 in proteoliposomes to achieve high purity and to avoid
165 background signals from wheat-germ expression reagents. Both Coomassie Brilliant
166 Blue (CBB) staining and western blotting detected a 35 kDa band for PfLPLAT1 and
167 a faint band at higher molecular weight (approximately 55 kDa), which might be
168 dimerized PfLPLAT1 or complexed with other proteins (Fig. 2B). After purification,
169 PfLPLAT1 was reacted with 6 acyl-CoAs (16:0-, 18:0-, 18:2-, 20:4-, 20:5- and 22:6-
170 CoA) and each deuterium-labeled LPL (d9-LPA(16:0), d31- LPC(16:0), or d9-
171 LPE(16:0)) to produce diacyl phospholipid products PAs, PC, and PEs). Deuterated
172 LPLs enabled us to distinguish newly synthesized lipids from residual lipids of the
173 same type. In a given substrate-rich condition, six deuterated PAs, four PCs, and faint
174 activity for PE were detected (Fig. 2C, D, and E). In all PA products, PA(34:2) and
175 PA(36:5) were the most abundant, showing that PfLPLAT1 utilized linoleic acids (18:2-
176 CoA) and eicosapentaenoic acids (20:5-CoA) as acyl chain donors. These acyl-CoA
177 moieties were also used and produced PC(34:2) and PC(36:5). As for saturated and
178 monounsaturated lipids, PfLPLAT1 used16:0-CoA and 18:1-CoA as donors for both
179 LPA and LPC to a slightly lower extent. Taken together, this enzyme assay revealed
180 that PfLPLAT1 could utilize LPAs and LPCs as its substrates and may prefer to use
181 polyunsaturated fatty acids in the PA production.
182

183 **PfLPLAT1 is essential in asexual replication and stage transition of *P.***
184 ***falciparum***

185 To study the role of *Pflplat1* in the asexual life cycle of parasites, we generated
186 conditional knockout parasite lines, which were referred to as *Pflplat1*:LoxPint:HA,
187 using the dimerizable Cre recombinase (DiCre) system[27,28]. We incorporated the
188 plasmid DNA targeting native *Pflplat1* locus with the selection-linked integration (SLI)
189 method[29] (Fig 3A) and confirmed the integration by a diagnostic PCR (Fig 3B and Fig
190 S1A). To check whether the conditional knockout system works in established parasite
191 lines, PCR, western blotting, and indirect immunofluorescence assay (IFA) were
192 performed (Fig 3C–E and Fig S1B–D). Shifts in DNA bands were observed in
193 rapamycin-treated *Pflplat1*:LoxPint:HA C9 and G6 clonal lines, which indicated that
194 *Pflplat1* locus flanked by LoxP sites was excised and shortened (Fig 3C and Fig S1B).
195 Western blotting analysis revealed decreased protein expression of PfLPLAT1 after
196 24 hours (fractional decrease in band density: 72.2% ± 11.2 (C9), 59.8% ± 25.1 (G6))
197 or 48 hours (95.9 ± 3.12 (C9), 91.3 ± 4.89 (G6)) of rapamycin treatment (Fig 3D and
198 Fig S1C). Moreover, IFA showed a significant decrease in the immunofluorescence
199 intensity of PfLPLAT1 after 24 hours of rapamycin treatment (Fig 3E and Fig S1D).
200 Taken together, *Pflplat1* was efficiently knocked out in transgenic parasites in the
201 presence of rapamycin.

202 To study the effect of *Pflplat1*-defect on the asexual replication of parasites, we
203 performed growth assays using synchronized *Pflplat1*:LoxPint:HA C9 and G6 clonal
204 lines. The parasitemia of rapamycin-treated (+Rap) parasites did not increase and
205 recover until the end of assay, while that of rapamycin-untreated (−Rap) parasites
206 showed normal growth (Fig 3F). This clearly indicated that *Pflplat1* is essential for
207 parasite growth in the erythrocytic stages, which is concordant with the low
208 mutagenesis index score of *Pflplat1* shown in previous genome wide screening[30].
209 *Pflplat1*:LoxPint:HA C9 clonal line was used in further analyses because no obvious
210 differences in gene knockout efficiency and growth kinetics between two parasite
211 clones were observed in the presence of rapamycin. To test if the growth defect of
212 rapamycin-treated *Pflplat1*:LoxPint:HA was due to the ablation of *Pflplat1,* we
213 established a genetically complementary line, *Pflplat1*:LoxPint:HA^{comp}, expressing
214 episomal PfLPLAT1 (Fig 3G). Growth assays of this parasite line showed that +Rap
215 parasites were able to grow to the same extent as rapamycin-nontreated parasites,
216 which indicated that aberrant growth of +Rap *Pflplat1*:LoxPint:HA was due to the lack
217 of PfLPLAT1 (Fig 3G). Analyses of stage distribution of *Pflplat1*:LoxPint:HA with or
218 without rapamycin treatment revealed clear differences in their stage at 36 hours post-
219 infection (hpi) (Fig 3H). −Rap parasites entered into the schizont stage at 36 hpi, while
220 +Rap parasites did not exhibit cell division. The growth of +Rap parasites was stalled

221 in the trophozoite stage when observed at 44 and 48 hpi. Moreover, shrunk and
222 pyknotic parasites were observed in the +Rap group at 44 hpi and approximately 50%
223 of parasites were found in the aberrant form at 48 hpi. This suggests that *Pflplat1* is
224 indispensable for stage transition from trophozoites to schizonts.

225 Previous transcriptional analyses showed that *Pflplat1* is highly expressed in the
226 gametocyte stage[31], which encouraged us to investigate the essentiality of *Pflplat1* at
227 this stage. Parasites were treated with rapamycin at day 10 after gametocytogenesis,
228 and gametocytemia was measured on days 12–15 post-gametocytogenesis. Although
229 *Pflplat1* was excised in the presence of rapamycin (Fig S2A), +Rap and −Rap
230 parasites showed no significant difference in gametocytemia and gametocyte stage
231 distribution (Fig S2B, S2C). This suggests that *Pflplat1* is not essential in the
232 maturation process of gametocytes.

233

234 **PfLPLAT1 colocalizes with endoplasmic reticulum throughout the asexual stage**

235 It was shown that most enzymes functioning in phospholipid synthesis were
236 integrated into the endoplasmic reticulum (ER) membrane in mammalian cells[32]. To
237 investigate whether PfLPLAT1 localizes on the ER, we performed an indirect IFA co-
238 stained with an ER marker protein BiP (binding immunoglobulin protein) and confocal
239 microscopy. Signal profiles of PfLPLAT1 and BiP showed similar patterns throughout

240 all asexual stages, which suggests that most PfLPLAT1 localizes on the ER (Fig 4,
241 right panel). In early and middle schizont stages, PfLPLAT1 and BiP were highly co-
242 localized based on the Pearson's r values (Fig 4, right panel). These two stages also
243 showed expression peaks of PfLPLAT1 and BiP[33]. Our results indicated that the ER
244 is a fundamental platform for phospholipid synthesis in *P. falciparum*, and demand for
245 phospholipids by parasites possibly reaches the highest level in the early and middle
246 schizont stages, in which parasites undergo multiple nuclear divisions.
247
248 ***Pflplat1* deletion caused abnormal cytostome formation and their internalization**
249 Our previous studies showed that mammalian LPLATs maintain the integrity of cellular
250 membranes in various tissues and their functions[15,16]. To study the effect of PfLPLAT1
251 deletion on the membrane morphology of parasites, we observed parasitized
252 erythrocyte structure at 36 hpi using a high-voltage scanning electron microscope (HV-
253 STEM), which enables sample sections of 250–1,000 nm thickness with 1000 keV
254 accelerating voltage to be obtained[34,35]. Due to the deeper penetration of electrons
255 into the target specimen, HV-STEM provides more representative images of
256 subcellular structures within a space. Sections (250 nm thickness) of rapamycin-
257 treated parasites showed gigantic omega-shaped and open-mouthed vacuoles (Fig
258 5C-K); such a structure was not observed in −Rap parasites (Fig 5A and B). These

259 vacuoles showed the typical characteristics of cytostomes, which comprise double
260 membranes (Fig 5H) derived from the parasite plasma membranes (PPMs) and
261 parasitophorous vacuole membranes (PVMs) and collars around the opening[36-38].
262 Although cytostomes with a normal appearance (diameter of approximately 190 nm)
263 were also observed in +Rap samples (Fig 5J)[39], the outer diameter of abnormal
264 cytostomes reached approximately 500 nm (Fig 5F and K). Furthermore, several
265 vacuoles were observed between PPM and PVM in *Pflplat1*-deficient parasites (Fig
266 5G), which may be transported from either side of the PPMs and PVMs.

267 *P. falciparum* acquires hemoglobin and other nutrients through the cytostome and
268 digests hemoglobin into amino acids in digestive vacuoles. Therefore, we
269 hypothesized that failures of fissions of cytostomes could lead to decreased
270 hemoglobin uptake and reduced size of hemozoins, which are crystalline products of
271 degraded hemoglobin. We quantified the size of hemozoins using polarized light
272 microscopy[40], which identify hemozoins with a high sensitivity due to the birefringence
273 caused by crystalline arrangements of β-hematin. In rapamycin-treated parasites at
274 30 hpi, the size of hemozoins was significantly decreased compared with that of
275 rapamycin-nontreated parasites (Fig S3). These findings support our hypothesis and
276 indicate that *Pflplat1*-deficiency leads to an insufficient supply of nutrients and amino
277 acids in parasites through the formation of abnormal cytostomes.

278

279 **Transcriptomic profiles reveal decreased gene expression related to DNA**

280 **replication and cell cycle regulation in *Pflplat1*-deficient parasites**

281 To explore biological mechanisms that cause the death of *Pflplat1*-deficient

282 parasites at the late-trophozoite stage, we studied the transcriptomes of +Rap and

283 −Rap *Pflplat1*:LoxPint:HA lines with samples collected at 24 and 30 hpi: timepoints

284 before the appearance of dying parasites. Although few differentially expressed genes

285 (DEGs) were detected at 24 hpi (Fig S4, Table S2) and the gene expression patterns

286 were not well clustered together in +Rap or −Rap samples (Fig S4), 267 upregulated

287 genes ($\log_2$FC > 0.5, adjusted p-value < 0.5) and 331 downregulated genes ($\log_2$FC <

288 0.5, adjusted p-value < 0.5) were observed at 30 hpi (Fig 6A, Table S2). The gene

289 expression profiles of +Rap or −Rap parasites at 30 hpi were well clustered together,

290 indicating sufficient reproducibility of gene expression analysis at this time point (Fig

291 S4). It was shown that 107 of 267 upregulated genes were classified as *Plasmodium*

292 interspersed repeat genes, almost all of which are highly expressed at the early

293 trophozoite stage[31,33]. This result indicates the possibility that *Pflplat1*-deficiency leads

294 to delayed gene expression in +Rap parasites. Three hundred thirty-one

295 downregulated genes were shown to function in various biological process such as

296 the lipid metabolic pathway, DNA replication, GPI (glycosylphosphatidylinositol)

297 anchor biosynthetic process, metal ion transport, and the ERAD (ER-associated
298 degradation) pathway (Fig 6B and 6C), suggesting that *Pflplat1* deficiency affects a
299 wide variety of metabolic pathways in parasites. Downregulated genes are categorized
300 into DNA replication, cell cycle, DNA metabolic process, cell cycle regulation, and
301 nuclear division, which might explain the growth arrest of *Pflplat1*-deficient parasites
302 at the late trophozoite stage (Fig 3H).
303

304 **Lipidomic analysis reveals the effect of PfLPLAT1 on lipid profiles of malaria**
305 **parasites**

306 To investigate the effect of PfLPLAT1 deletion on the profile of phospholipid species
307 in parasites, we performed a LC-MS/MS-based lipidomic analysis using +Rap and
308 −Rap *Pflplat1*:LoxPint:HA. Phospholipids were extracted from parasites at 30 hpi and
309 subjected to LC-MS/MS. In +Rap parasites, 9 of 10 PAs, 4 of 14 Pes, and 16 of 24
310 PCs but only 2 of 12 sphingomyelies (SMs) species were decreased compared with
311 those in −Rap parasites (Fig 7A–D). The sum of PA, PE, and PC decreased in +Rap
312 parasites, while that of SM did not change (Fig 7E). This indicates that PfLPLAT1 may
313 also have activity for producing diacyl forms of PA, PE, and PC in parasites, which is
314 partly consistent with the *in vitro* enzymatic activity of PfLPLAT1 (Fig 2C–E).
315 Furthermore, the relative amount of PA(32:0), PA(34:0), PA(34:1), PC(36:5), and

316 SM(42:3) was decreased, whereas that of PA(34:2) and PC(31:0) was increased in

317 +Rap parasites (Fig S5). Collectively, *Pflplat1* deficiency led to decreased amounts of

318 phospholipids and affected these phospholipid compositions in parasites.

319 **Discussion**

320 Phospholipids are *de novo* synthesized in the Kennedy cycle,[9] and acyl chains of
321 these phospholipids can be exchanged by phospholipase A2 and LPLATs in the Lands
322 cycle[10]. This process maintains phospholipid diversity in tissues for their function. More
323 than 14 LPLATs are known to function in these cycles, and several LPLs are frequently
324 used as substrates by a single LPLAT[14]. In our enzyme assay, recombinant PfLPLAT1
325 expressed by a wheat germ *in vitro* expression system showed high specificity against
326 LPAs and a mild preference for LPCs as acyl chain acceptors. This finding highlighted
327 that PfLPLAT1 functions not only as an LPAAT but also as an LPCAT, showing that
328 *P. falciparum* may also undergo the Lands cycle pathway. A previous bioinformatic
329 analysis suggested that there are 26 phospholipases encoded by the parasite's
330 genome[41,42], while PfLPLAT1 described in this report is one of a few entries we
331 identified from our database search. In contrast to the multiple LPLATs and
332 phospholipases involved in the Lands cycle, *P. falciparum* may have a few LPLATs,
333 which in turn suggests that PfLPLATs may be critical for the regulation of phospholipid
334 biosynthesis. We are still characterizing other putative PfLPLATs regarding their
335 enzymatic activities, but, considering the limited possibility of PfLPLATs and that
336 PfLPLAT1 is an essential enzyme, parasite LPLATs might have activity against

337 multiple LPL species in addition to LPA and LPC to control the optimal profile of lipid
338 species for parasite cell homeostasis.

339 PfLPLAT1 preferentially uses unsaturated fatty acids such as linoleic acids and
340 eicosapentaenoic acids as substrates (Fig 2C and D). Lipids with unsaturated fatty
341 acids have larger molecular cross-sectional areas that may ease molecular packing
342 and increase membrane flexibility. This indicates that PfLPLAT1 helps the parasite
343 plasma membrane to maintain a high flexibility and/or low viscosity to deal with acute
344 deformations of the parasite membrane during its rapid replication.

345 While fatty acid synthesis, neutral lipid storage, cholesterol transport, and
346 phospholipase studies in parasites have progressed, development of a
347 comprehensive understanding of the phospholipid synthesis pathway remains
348 insufficient. Several transgenic parasites to conditionally target essential genes related
349 to lipid metabolism have been established, and their growth kinetics were studied upon
350 induction of gene deletion[41,43-46]. However, the growth defects of gene-deficient
351 parasites were observed only after several cycles had passed, in contrast to the
352 obvious growth abnormality detected in *Pflplat1*-deficient parasites at the first cycle.
353 This result indicates that the PfLPLAT itself and/or downstream of lipid maintenance
354 in the parasite is highly important for their normal growth.

355 Abnormal cytostomes in *Pflplat1*-deficient parasites occurred during the course of
356 parasite death, which has not been reported in previous studies. Cytostomes occur in
357 a clathrin-independent manner in *P. falciparum*,[47] and dynamin-like protein 1
358 (PfDYN1) does not localize on the collars of cytostomes[48]. Moreover, PfDYN1 and
359 PfDYN2 were not identified as downregulated genes in our transcriptomic analysis
360 (Fig. 6), suggesting that PfDYNs are likely independent of the formation of abnormal
361 cytostomes, regardless of their ability to pinch off the membrane. Our EM data showed
362 that abnormal cytostomes had large openings that were at least three times the
363 diameter of normal cytostomes. This indicates that the physical states of the openings
364 with negative membrane curvature are different from those of normal cytostomes. PA
365 and PE have molecular shapes of inverted cones and generate negative curvature,
366 which leads to efficient vesicle fusions, fissions[49,50], and cytokinesis in mammalian
367 cells[51]. Considering these physical properties of PA, as well as the reduced levels of
368 PA, PE, and PC, it is reasonable to speculate that lipid profile changes in *Pflplat1*
369 deficiency could interrupt cytostome fission and lead to the formation of gigantic
370 vesicles due to PA shortage in the cell membrane (Fig. 8). Downregulation of *P.*
371 *falciparum* homolog of vesicle-associated membrane protein 8 (VAMP8), a SNARE
372 protein on lysosomes, in *Pflplat1*-deficient parasites also may drive further
373 abnormalities. VAMP8 regulates lysosome–autophagosome associations[52,53] and

374 SNARE proteins are proposed to function in cytostome-digestive vacuole (DV) fusion[48].
375 Thus, dysregulation of cell membrane curvature and fusion of cytostomes with DVs by
376 downregulated VAMP8 possibly leads to abnormal hemoglobin digestion in a
377 coordinated manner (Fig. 8).

378 In mammals and yeasts, the cell cycle is rigorously regulated by mitotic kinases,
379 including cyclin-dependent kinases (CDK), polo-like kinases, aurora kinases, NIMA-
380 related kinases (NEK), protein phosphatases, and RING E3 ubiquitin ligases[54]. *P.*
381 *falciparum* has some homologs of these proteins despite its tendency to become
382 asynchronous with membrane-intact nuclear divisions followed by cytokinesis to
383 separate multiple nuclei. Our transcriptomic analysis showed that PfCyc2, CDK-
384 associated proteins, protein kinase 5 (PfPK5), and PfNEK3 were downregulated in
385 *Pflplat1*-deficient parasites. Although the functions of most of these kinases remain
386 unknown, PfPK5 was shown to be important for progression of parasites to the
387 schizont stage through phosphorylation of origin recognition complex subunit 1
388 (PfORC1), a component of the pre-replication complex (pre-RC)[55]. Interestingly,
389 *Pflplat1*-deficient parasites showed similar transcriptome profiles to those of dormant
390 parasites, whose expression of pre-RC components (minichromosome maintenance
391 complex component 5 (PfMCM5) and origin recognition complex subunit 4 (PfORC4))
392 and DNA mismatch repair proteins is decreased[56]. Therefore, *Pflplat1* deficiency may

393 decrease the expression of pre-RC components and mitotic kinases, which retards the
394 assembly of pre-RC and also prevents the disassembly of pre-RC. These phenomena
395 might sequester parasites into the trophozoite stage and lead to the termination of
396 cellular activities in parasites.
397

398 **Conclusion**

399 Lipid metabolism and related areas in malaria parasites have been attractive for
400 researchers as new study areas as well as potential drug targets[2]. Multi-membrane
401 structures of infected erythrocytes and trafficking of both lipid and proteins are
402 supported by lipid metabolism with a strict balance and molecular flux between
403 organelles. Our study on PfLPLAT1 sheds light on the importance of the phospholipid
404 synthesis pathway, particularly PA as an essential substance for the cell cycle
405 progression of parasites. Considering our database search returned only a few entries
406 that have sequence similarities, and PfLPLAT1 is an essential gene, other
407 acyltransferases yet to be identified would function differently from PfLPLAT1 if they
408 exist, but their roles should orchestrate each other to maintain normal cell cycle
409 progression and parasitized erythrocyte structure.

410 **Methods**

411 **Parasite culture**

412 *Plasmodium falciparum* NF54::DiCre strain (kindly gifted from Moritz Treeck) was
413 cultured in O^+ erythrocytes at 5% hematocrit in RPMI-1640 media (Thermo Fisher
414 Scientific, Waltham, MA, USA) supplemented with 5.95 mg/mL HEPES, 0.05 mg/mL
415 hypoxanthine (Merck, Darmstadt, Germany), 2 mg/mL sodium bicarbonate (FUJIFILM
416 Wako Chemical Corporation, Kanagawa, Japan), 10 µg/mL gentamicin (Thermo
417 Fisher Scientific), and 0.5% Albumax II (Thermo Fisher Scientific) (RPMI-1640
418 complete media) and maintained at 37°C in a gas mixture of 5% O_2 , 5% CO_2 and 90%
419 N_2, as previously described[7]. The experiments with human erythrocytes were
420 conducted under the guidelines of the ethics committee of Nagasaki University
421 (#191226226). Human erythrocytes were obtained from the Japan Red Cross Society
422 (Tokyo, Japan) (No: R030027).

423

424 **Generation of *Pflplat1*:LoxPint:HA line**

425 To conditionally knockout *Pflplat1*, we generated pSLI-*Pflplat1*-LoxP-3×2A-HA
426 plasmid to introduce LoxP sites into *Pflplat1* utilizing a selection-linked integration (SLI)
427 method[29]. To create pSLI-*Pflplat1*-LoxP-3×2A-HA, Pfef1a-5'UTR-pD3HA[57] was
428 linearized at BglII and XmaI restriction sites. Synthetic DNA containing a LoxP site

429 followed by 3′ recodonized *Pflplat1*, triple influenza hemagglutinin (HA) sequences, a
430 2A self-cleaving peptide sequence, a neomycin resistance gene cassette, a LoxP site,
431 and a GFP reporter gene was obtained (Azenta Life Sciences, Burlington, MA, USA).
432 5' genomic *Pflplat1* was amplified from the genomic DNA of NF54::DiCre strain with
433 CloneAmp HiFi PCR Premix (Takara Bio, Shiga, Japan) using primers listed in Table
434 S1. These sequences were introduced into linearized Pfef1a-5'UTR-pD3HA using an
435 In-Fusion HD Cloning Kit (Takara Bio).
436 For plasmid DNA transfection of pSLI-*Pflplat1*-LoxP-3×2A-HA, trophozoite and
437 schizont-stage parasites were collected with MACS magnetic columns (Miltenyi Biotec,
438 Bergisch Gladbach, Germany). RBCs were electroporated in cuvettes (Bio-Rad,
439 Hercules, CA, USA) with the plasmid using a GenePulser Xcell (Bio-Rad). Collected
440 parasites were incubated with electroporated RBCs in RPMI-1640 complete medium
441 for 48 hours. After 48 hours, parasites were selected with 1 nM WR99210 (Merck) for
442 3–4 weeks followed by 400 μg/mL G418 (FUJIFILM Wako Pure Chemical
443 Corporation) for 2 weeks. Limiting dilutions were performed using selected
444 transgenic parasites to obtain clonal parasites. To confirm plasmid integration in the
445 genome of clonal parasites, genomic DNA was extracted using a DNeasy Blood &
446 Tissue Kit (QIAGEN, Venlo, Netherlands) and a diagnostic PCR was performed using
447 the primers listed in Table S1.

448

449 **Generation of *Pflplat1*:LoxPint:HA^{comp}**

450 To generate the *Pflplat1* genetically complimentary line (*Pflplat1*:LoxPint:HA^{comp})
451 from the *Pflplat1*:LoxPint:HA C9 line, we created a p*hsp86-Pflplat1*-myc rescue
452 plasmid. To remove Cas9 coding sequence from pUF-Cas9-pre-sgRNA (Addgene
453 plasmid #137845; http://n2t.net/addgene:137845; RRID:Addgene_137845), the
454 plasmid was linearized at the XhoI and SalI restriction sites. Synthetic DNA containing
455 *Pflplat1* coding sequence followed by sequences of linker and triple c-myc was
456 obtained (Azenta Life Sciences). These sequences were introduced into linearized
457 pUF-Cas9-pre-sgRNA using an In-Fusion HD Cloning Kit (Takara Bio).

458 For plasmid DNA transfection of p*hsp86-Pflplat1*-myc, trophozoite and schizont-
459 stage *Pflplat1*:LoxPint:HA C9 were collected with MACS magnetic columns (Miltenyi
460 Biotec). RBCs were electroporated in cuvettes (Bio-Rad) with the plasmid using a
461 GenePulser Xcell (Bio-Rad). Collected parasites were incubated with electroporated
462 RBCs in RPMI 1640 complete medium for 48 hours. After 48 hours, parasites were
463 selected with 500 nM DSM-1 (Merck) for 3–4 weeks. To confirm that PfLPLAT1 was
464 episomally expressed in *Pflplat1*:LoxPint:HA^{comp}, we performed western blotting.

465

466 **Multiple sequence alignment of LPAATs**

467 For multiple alignment of LPAAT sequences, the amino acid sequences were
468 obtained from the NCBI database (https://www.ncbi.nlm.nih.gov/) (*Plasmodium*
469 *falciparum* (*P. falciparum*) LPLAT1, XP_001348595.2; *Homo sapiens* (*H. sapiens*)
470 LPLAT1, NP_001358367.1; *Mus musculus* (*M. musculus*) LPLAT1, AAB82009.1;
471 *Caenorhabditis elegans* (*C. elegans*) ACL-1, CAB03160.1; *Saccharomyces cerevisiae*
472 (*S. cerevisiae*) SLC1, NP_010231.1; *Toxoplasma gondii* (*T. gondii*), XP_002366705.1;
473 *Babesia bovis* (*B. bovis*), XP_001610213.1; *Plasmodium yoelii* (*P. yoelii*) PY01678,
474 XP_729473.2; *P. yoelii* PY02486, XP_730369.1; *Trypanosoma brucei* (*T. brucei*),
475 XP_829573.1; *Escherichia coli* (*E. coli*), AAA24397.1). The alignment was performed
476 using CLUSTALW (v2.1). Sequence logos were created using WebLogo (v2.8.2).
477

478 **Estimation of the three-dimensional structure of PfLPLAT1 and *Hs*AGPAT1**

479 For three-dimensional construction of these enzymes, Protein Data Bank files were
480 obtained from the AlphaFold Protein Structure Database (https://alphafold.ebi.ac.uk/)
481 (PfLPLAT1; AF-Q8IL28-F1-model_v4, *Hs*AGPAT1; AF-Q99943-F1-model_v4). The
482 three-dimensional structure was visualized using PyMoL (v0.99rc6).
483

484 **Growth assay**

485 For growth assays, parasites were synchronized with 5% D-sorbitol (FUJIFILM
486 Wako Pure Chemical Corporation) and seeded in 24-well plates. Synchronized
487 parasites were cultured in 1 mL RPMI-1640 complete medium at 5% hematocrit and
488 incubated with rapamycin (100 nM; Merck) or an equivalent volume of dimethyl
489 sulfoxide. Parasitemia was counted every day using a Sysmex XN-30 hematology
490 analyzer (Sysmex Corporation, Kobe, Japan)[58] and kept lower than 5% by serial
491 passages. The membranes of parasitized erythrocytes were permeabilized using
492 CELLPACK DCL (Sysmex Corporation), and nucleic acids of parasites were stained
493 using Fluorocell M (Sysmex Corporation) and Lysercell M (Sysmex Corporation).
494 Growth curves were depicted using GraphPad Prism (v8.4.3) (GraphPad Software,
495 Boston, MA, USA).
496

497 **Quantification of parasite stage distribution**

498 For quantification of parasite stage distribution, trophozoite- and schizont-stage
499 parasites were collected with MACS magnetic columns (Miltenyi Biotec). Collected
500 parasites were incubated at 2% hematocrit in RPMI-1640 complete medium for 4
501 hours in agitated conditions (rotated at 40 rpm) to remove multiple infections of
502 parasites in a single RBC. After 4 hours of incubation, parasites were tightly
503 synchronized with 5% D-sorbitol (0-4 h post invasion) and seeded in six-well plates.

504 Blood films were created at each time point and stained with Giemsa′s azur eosin
505 methylene blue solution (Sigma–Aldrich, Burlington, MA, USA). Stage counting was
506 performed manually under a light microscope.
507
508 **Immunofluorescence assay**
509 Infected RBCs were immobilized on coverslips (Thorlabs, Inc., Newton, NJ, USA)
510 coated with poly-D-lysine (MP Biomedicals, Santa Ana, CA, USA). After the
511 immobilization, samples were fixed with 4% paraformaldehyde (Electron Microscopy
512 Sciences, Hatfield, PA, USA) in phosphate buffered saline (PBS) for 10 min and 50
513 mM dimethyl suberimidate dihydrochloride (Sigma–Aldrich) in borate buffer for 20 min,
514 followed by quenching with 10 mM glycine in PBS for 30 min. Fixed samples were
515 permeabilized with 0.3% Triton X-100 (FUJIFILM Wako Pure Chemical
516 Corporation) in PBS and blocked with 1% skim milk in 0.05% Tween 20 (Tokyo
517 Chemical Industry Co., Ltd., Tokyo, Japan) in PBS for 60 min. Samples were treated
518 with primary antibodies overnight and secondary antibodies for 60 min, followed by
519 sealing with VECTASHIELD Antifade Mounting Medium with DAPI (Vector
520 Laboratories, Inc., Newark, CA, USA). Mouse anti-HA antibody (6E2) (Cell Signaling
521 Technology, Danvers, MA, USA) was used at 1:50 dilution. Rabbit anti-BiP antibody
522 (MR4, Manassas, VA, USA) was used at 1:15 dilution. Alexa Fluor 488-conjugated

523 goat anti-mouse (Thermo Fisher Scientific, Carlsbad, CA, USA), Alexa Fluor 594-
524 conjugated goat anti-mouse, and Alexa Fluor 594-conjugated goat anti-rabbit
525 antibodies were used at 1:1000 dilution. Samples were observed with a 100× objective
526 using an LSM780 confocal laser scanning microscope (Carl Zeiss, Oberkochen,
527 Germany).
528 ZEN lite (v3.5) (Carl Zeiss) was utilized to quantify the intensity of
529 immunofluorescence signals in parasites. To plot signal profiles, the intensity on
530 drawing lines was measured using the Profile Plot analysis tool in ImageJ (v1.53t)
531 (https://imagej.nih.gov/ij/). For co-localization analysis, Pearson's r values were
532 calculated using the Coloc 2 tool in Fiji (v2.9.0) (https://imagej.net/software/fiji/).
533
534 **Western blotting**
535 For western blot analysis, parasites were collected with MACS magnetic columns
536 (Miltenyi Biotec) and lysed in 0.03% saponin solution for 5 min. Collected samples
537 were dissolved in lysis buffer (4% SDS, 0.5% Triton X-100, 25-75 U DNase I (Takara
538 Bio) and cOmplete protease inhibitor cocktail (Roche, Basel, Switzerland) in 0.5%
539 PBS) and denatured with SDS sample buffer containing protein-reducing agents
540 dithiothreitol. Lysates were boiled at 95°C for 3 min and run on polyacrylamide gels
541 (Thermo Fisher Scientific). Proteins were transferred on PVDF membranes and

542 blocked with a Bullet Blocking One (nacalai tesque, Kyoto, Japan). Blocked
543 membranes were incubated with primary antibodies for 1 hour followed by secondary
544 antibodies conjugated to horseradish peroxidase (HRP) (Jackson ImmunoResearch
545 Laboratories Inc., West Grove, PA, USA) for 30 min. Mouse anti-HA antibody (6E2)
546 (Cell Signaling Technology, Inc., Danvers, MA, USA) was used at 1:1000 dilution.
547 Mouse anti-Myc antibody (9B11) (Cell Signaling Technology) was used at 1:1000
548 dilution. Mouse HRP was used at 1:5000 dilution. After probing with antibodies, the
549 membranes were incubated with chemiluminescent HRP substrate (Thermo Fisher
550 Scientific) for 5 min and proteins were visualized with WSE-6100 LuminoGraph I
551 (ATTO, Tokyo, Japan). To investigate the protein expression levels of PfAldolase as
552 an internal control, the membrane was washed with WB Stripping Solution Strong
553 (nacalai tesque) for 30 min and blocked with Bullet Blocking One. After blocking, the
554 membrane was incubated with HRP anti-plasmodium aldolase antibody (1:2000;
555 Abcam, Cambridge, UK) for 30 min and chemiluminescent HRP substrate (Thermo
556 Fisher Scientific) for 5 min.
557
558 **Gametocytogenesis**
559 For gametocytogenesis, the parasite was maintained at 6% hematocrit in RPMI
560 complete medium with 10% human serum (#28J0058; Japan Red Cross) and

561 parasitemia was adjusted to 0.1%, as previously decribed[7] (day 1). Hematocrit was
562 reduced to 3% on day 4. The parasite was treated with 50 mM N-acetyl glucosamine
563 (Sigma–Aldrich) to remove asexual parasites on days 9–11 and treated with 100 nM
564 rapamycin (Sigma–Aldrich) from day 10. Giemsa-stained blood films were created to
565 count gametocytemia and to investigate stage distribution of gametocytes manually
566 on days 12–15. Media were replaced with pre-warmed and fresh medium every day
567 up to day 15. For extraction of genomic DNA from the gametocyte, it was separated
568 into an interface between layers of 40% and 60% Percoll and collected with MACS
569 magnetic columns (Miltenyi Biotec) on day 14. Genomic DNA was extracted using a
570 DNeasy Blood & Tissue Kit (Qiagen) and PCR was performed using the primers listed
571 in Table S1.
572
573 **Transcriptomic analysis**
574 For purification of RNA, parasites were collected with MACS magnetic columns
575 (Miltenyi Biotec). Collected parasites were incubated at 2% hematocrit in RPMI-1640
576 complete medium for 4 hours in agitated conditions (rotated at 40 rpm) to remove
577 multiple infections of parasites with a single RBC. After 4 hours of incubation, parasites
578 were tightly synchronized with 5% D-sorbitol (0–4 h post invasion) and returned to
579 RPMI-1640 complete medium with or without 100 nM rapamycin. Infected RBCs were

580 harvested at 24 and 30 hours post-infection and dissolved in TRIzol Reagent (5 times
581 the volume of RBCs) (Thermo Fisher Scientific). Dissolved samples were stored at
582 −80°C until purification of RNA. RNA was separated from samples using Phasemaker
583 Tubes (Thermo Fisher Scientific) and purified using a PureLink RNA Mini Kit (Thermo
584 Fisher Scientific).

585 mRNAs were isolated from total RNAs using poly-T oligo-attached magnetic beads.
586 For construction of a directional library, first-strand cDNA was synthesized using
587 random hexamer primers and second-strand cDNAs were synthesized using dUTPs
588 after fragmentation of captured mRNAs. After synthesis of double-stranded cDNA, end
589 repair of double-stranded cDNA, 3'-adenylation (A-tailing), adapter ligation, size
590 selection, USER enzyme excision, PCR amplification, and purification were performed.
591 Real-time PCR and Qubit (Thermo Fisher Scientific) were utilized for quantification of
592 the libraries. Quantified libraries were sequenced using Illumina Novaseq 6000
593 (Illumina Inc., San Diego, CA, USA). Raw data (raw reads in fastq format) were
594 processed through in-house Perl scripts to remove reads containing adapters and
595 ploy-N and reads with low quality. Paired-end reads were aligned to the reference
596 genome (release-42 of *P. falciparum* 3D7) using Hisat2 (v2.0.5). Counting of the
597 number of reads mapped to each gene was performed using FeatureCounts (v1.5.0).
598 Differential expression analysis was performed using edgeR (v3.43.7). Adjusted p-

599 values were calculated using the Benjamini–Hochberg method. Gene Ontology
600 enrichment analysis of DEGs was performed using clusterProfiler (v4.9.1). The
601 hypergeometric test was performed to calculate p-values.
602
603 **Hemozoin quantification**
604 For quantification of hemozoin, parasites were collected with MACS magnetic
605 columns (Miltenyi Biotec). Collected parasites were incubated at 2% hematocrit in
606 RPMI 1640 complete medium for 4 hours in agitated conditions (rotated at 40 rpm) to
607 remove multiple infections of parasites with a single RBC. After 4 hours of incubation,
608 parasites were tightly synchronized with 5% D-sorbitol (0-4 h post invasion) and
609 returned to RPMI-1640 complete medium with or without 100 nM rapamycin. Infected
610 RBCs were observed under a Leica DMi8 inverted microscope (Leica Microsystems,
611 Wetzlar, Germany) and exposed to polarized light to visualize hemozoins. The area of
612 reflected lights (indicators of hemozoins) was measured using the Analyze Particle
613 tool in ImageJ (v1.53t) (https://imagej.nih.gov/ij/).
614
615 **Sample preparation for transmission electron microscopy (TEM) and scanning**
616 **transmission electron microscopy (STEM)**

617 Sample preparation for TEM samples was slightly modified from previous papers
618 [59,60]. Briefly, the trophozoite and schizont stages of +Rap and −Rap parasites purified
619 by MACS LS columns (Miltenyi Biotec.) were collected by centrifugation at 1300 × *g*
620 for 5 min. These parasitized erythrocytes were fixed with 2% glutaraldehyde (Electron
621 Microscopy Sciences) with 2% paraformaldehyde (Electron Microscopy Sciences) and
622 1% tannic acid (Merck) in 0.1 mol/L cacodylate buffer (TAAB Laboratories Equipment
623 Ltd., Aldermaston, Berks, England), pH 7.4. Erythrocytes were further fixed with 1%
624 osmium tetroxide aqueous solution (Electron Microscopy Sciences) for 1 hour at 4°C.
625 Erythrocyte pellets were washed three times with ultrapure water, embedded in 2%
626 agarose (PrimeGel Agrose LMT, Takara) when necessary, stained with 2% uranyl
627 acetate (Electron Microscopy Sciences) on ice for 1 hour, and washed three times with
628 ultrapure water.
629 The samples were serially dehydrated with 50%, 70%, 80%, 90%, 95%, and 100%
630 ethanol for 10 min each. Infiltration of propylene oxide (FUJIFILM Wako Pure
631 Chemical Corporation) was performed for 50 min at room temperature. Samples were
632 embedded in propylene oxide with resin mixture; (23.8 mL Quetol-812, 11.2 mL DDSA,
633 15 mL MNA, and 0.9 mL DMP-30; Nisshin EM, Tokyo, Japan; 1:1 volume ratio)
634 overnight. The samples were then heated for 30 hours at 60°C. Thick sections
635 (approximately 250 nm) were generated with a diamond knife (DiATOME, Biel,

636 Switzerland). After collecting sections by 200 mesh copper grids (GILDER GRID,
637 No100; Gilder Grids Ltd., Grantham, Lincolnshire, UK), specimens were stained with
638 5% uranyl acetate solution (Merck) plus 0.4% lead citrate (TABB Laboratories
639 Equipment Ltd), and then osmium coating was applied for observation by STEM (JEM-
640 1000K RS, JEOL Ltd., Tokyo, Japan).
641

642 **Measurement of PfLPLAT1 enzymatic activities**

643 To identify the specificities of both LPLs and acyl chain donors, 2 μg
644 proteoliposomes was mixed with 25 μM of one type of deuterated LPLs (16:0-d9 LPA,
645 16:0-d31 LPC, or 16:0-d9 LPE) and a mixture of 1 μM fatty acid CoAs (16:0-CoA, 18:1-
646 CoA, 18:2-CoA, 20:4-CoA, 20:5-CoA, and 22:6-CoA) in 100 mM Tris HCL (pH 7.4), 1
647 mM EDTA, and 2 mM $CaCl_2$ (total reaction volume of 100 μL). The mixtures were
648 incubated at 37ºC for 30 min and the enzyme reaction was stopped by adding 500 μL
649 MeOH. The samples were centrifuged, and the supernatants were transferred to new
650 tubes.

651 The deuterated product diacyl phospholipids were detected by mass spectrometry
652 and quantified based on the signal intensities of external standards for each lipid type
653 (PC(34:1), PE(34:1), and PA(34:1)).

654 To prepare samples for lipid profile analyses, trophozoites and schizonts were
655 separated by LS magnetic columns (Miltenyi Biotec), and further synchronized by
656 incubating for 4 hours after mixing with 10 times the volume of non-parasitized
657 erythrocytes and 5% sorbitol treatment. The number of cells were adjusted, and total
658 lipids were directly extracted by treating synchronized parasites with 40 times the
659 volume of MeOH.
660
661 **LC-MS analyses**
662 Evaluation of enzyme activity and phospholipid profiles in the parasitized
663 erythrocytes was performed by LC/ESI/MS/MS using a Nexera UHPLC system and a
664 triple quadrupole mass spectrometer LCMS-8060 (Shimadzu Corp., Kyoto, Japan). An
665 Acquity UPLC BEH C8 column (1.7 μm, 2.1 mm x 100 mm, Waters Corp., Milford, MA,
666 USA) was used for chromatographic separation with three phases: 5 mM
667 NH_4HCO_3/water (mobile phase A), acetonitrile (mobile phase B), and isopropanol
668 (mobile phase C). Column oven temperature was set at 47°C. To analyze the
669 enzymatic activity of PfLPLAT1 and PE and PC profiles in the parasitized erythrocytes,
670 the pump gradient [time (%A/%B/%C)] was programmed as follows: 0 min (75/20/5)-
671 20 min (20/75/5)-40 min (20/5/75)-45 min (5/5/90)-50 min (5/5/90)-55 min (75/20/5).
672 For analyzing the PA profile in the parasitized erythrocytes, the pump gradient [time

673 (%A/%B/%C)] was programmed as follows: 0 min (95/5/0)-8 min (70/30/0)-16 min
674 (30/35/35)-28 min (6/47/47)-35 min (6/47/47)-35.1 min (95/5/0). Injection volume was
675 5 μL. Column oven temperature was set at 47°C and the flow rate was 0.35 mL/min.
676 Multiple reaction monitoring transitions for phospholipids were set as follows: PC
677 ([M+H] →184.1, positive mode), PE ([M+H] →[M+H]–141, positive mode), PA ([M-H]
678 →153.1, negative mode), and SM ([M+H] →184.1, positive mode), where M is m/z of
679 molecular-related ions. LabSolutions LCMS software (Shimadzu Corp.) was used for
680 the operation of the equipment and data acquisition. Peak identifications and peak
681 area integrations were performed using TRACES
682 (https://github.com/KitaYoshihiro/TRACES)[61]. In profile analyses, area values of at
683 least 10,000 were considered as reliable numbers, and lipid species with area values
684 of more than 50,000 in the control groups were selected for the data analyses[61].
685

686 **Statistical analysis**

687 Data was checked for normality using the Shapiro–Wilk test. Statistical tests were
688 performed using R software (v4.3.1) (https://www.r-project.org) and GraphPad Prism
689 (v8.4.3).

690 **Data availability**

691 The RNA sequencing data have been deposited in DDBJ Sequence Read Archive

692 (DRA) (https://www.ddbj.nig.ac.jp/dra/index-e.html) as DRA017270.

693

694 **Acknowledgements**

695 We thank Dr. Moritz Treek (The Francis Crick Institute, UK) for providing
696 NF54::DiCre parasites for this study. We also thank Drs. Takao Shimizu (Institute of
697 Microbial Chemistry, Tokyo, Japan), Eizo Takashima (Ehime University, Ehime,
698 Japan), and Kazuhide Yahata (Ehime University, Ehime, Japan) for their helpful
699 discussions and technical advice. We are also grateful for the technical assistance in
700 high-voltage transmission electron microscopy and image analyses provided by Dr.
701 Shigeo Arai, Ms. Tomoyo, M.S., and Ms. Nakao Kahoru Yoda, B.S., of the High-
702 Voltage Electron Microscope Laboratory, Institute of Materials and Systems for
703 Sustainability, Nagoya University, Japan. This work was supported partially by Grants-
704 in-Aid for Scientific Research (KAKENHI) grant numbers: 17K08805 and 23K06518
705 (F.T.). The Department of Lipidomics, Graduate School of Medicine, University of
706 Tokyo, is supported by Shimadzu Corp. (Kyoto, Japan). The Department of Cellular
707 Architecture Studies, Institute of Tropical Medicine, Nagasaki University, is supported
708 by Shionogi and Co., Ltd. These funders were not involved in the design, experiments,
709 or data analyses for this study. Finally, we thank H. Nikki March, PhD, from Edanz
710 (https://jp.edanz.com/ac) for editing a draft of this manuscript.

711 **Author contributions**

712 Conceptualization: J.F., F.T., S.M., and H.S. Data collection: J.F., S.M.T., M.Y.,
713 E.S.H., J.U., and F.T. Data analysis: J.F., S.M.T., M.Y., E.S.H., T.S., D.K.I, J.U., H.S.,
714 and F.T. Funding acquisition: F.T. Supervision: K.K., J.U., H.S, and F.T. Writing –
715 original draft: J.F. and F.T. Writing – review & editing: J.F., S.M.T., M.Y., E.S.H., S.M.,
716 T.S., D.K.I., K.K., J.U., H.S., and F.T. Resources: F.T. and K.K.

Competing interests

No competing interests are declared.

References

1 Holz, G. G., Jr. Lipids and the malarial parasite. *Bull World Health Organ* **55**, 237-248 (1977).

2 Tokumasu, F., Hayakawa, E. H., Fukumoto, J., Tokuoka, S. M. & Miyazaki, S. Creative interior design by Plasmodium falciparum: Lipid metabolism and the parasite's secret chamber. *Parasitol Int* **83**, 102369, doi:10.1016/j.parint.2021.102369 (2021).

3 Vial, H. J., Eldin, P., Tielens, A. G. & van Hellemond, J. J. Phospholipids in parasitic protozoa. *Mol Biochem Parasitol* **126**, 143-154, doi:10.1016/s0166-6851(02)00281-5 (2003).

4 Ramakrishnan, S., Serricchio, M., Striepen, B. & Butikofer, P. Lipid synthesis in protozoan parasites: a comparison between kinetoplastids and apicomplexans. *Prog Lipid Res* **52**, 488-512, doi:10.1016/j.plipres.2013.06.003 (2013).

5 Iso, O. N. *et al.* Malaria Parasites Hijack Host Receptors From Exosomes to Capture Lipoproteins. *Front Cell Dev Biol* **9**, 749153, doi:10.3389/fcell.2021.749153 (2021).

6 Saeed, S., Tremp, A. Z. & Dessens, J. T. Plasmodium berghei oocysts possess fatty acid synthesis and scavenging routes. *Sci Rep* **13**, 12700, doi:10.1038/s41598-023-39708-z (2023).

7 Tanaka, T. Q. *et al.* Polyunsaturated fatty acids promote Plasmodium falciparum gametocytogenesis. *Biol Open* **8**, doi:10.1242/bio.042259 (2019).

8 Tokumasu, F., Crivat, G., Ackerman, H., Hwang, J. & Wellems, T. E. Inward cholesterol gradient of the membrane system in P. falciparum-infected erythrocytes involves a dilution effect from parasite-produced lipids. *Biol Open* **3**, 529-541, doi:10.1242/bio.20147732 (2014).

9 Kennedy, E. P. & Weiss, S. B. The function of cytidine coenzymes in the biosynthesis of phospholipides. *J Biol Chem* **222**, 193-214 (1956).

10 Lands, W. E. Metabolism of glycerolipides; a comparison of lecithin and triglyceride synthesis. *J Biol Chem* **231**, 883-888 (1958).

11 Harayama, T., Shindou, H., Ogasawara, R., Suwabe, A. & Shimizu, T. Identification of a novel noninflammatory biosynthetic pathway of platelet-activating factor. *J Biol Chem* **283**, 11097-11106, doi:10.1074/jbc.M708909200 (2008).

12 Yamashita, A. *et al.* Glycerophosphate/Acylglycerophosphate acyltransferases. *Biology (Basel)* **3**, 801-830, doi:10.3390/biology3040801 (2014).

754 13 Shindou, H., Eto, M., Morimoto, R. & Shimizu, T. Identification of membrane O-
755 acyltransferase family motifs. *Biochem Biophys Res Commun* **383**, 320-325,
756 doi:10.1016/j.bbrc.2009.04.013 (2009).
757 14 Valentine, W. J. *et al.* Update and nomenclature proposal for mammalian
758 lysophospholipid acyltransferases, which create membrane phospholipid
759 diversity. *J Biol Chem* **298**, 101470, doi:10.1016/j.jbc.2021.101470 (2022).
760 15 Iizuka-Hishikawa, Y. *et al.* Lysophosphatidic acid acyltransferase 3 tunes the
761 membrane status of germ cells by incorporating docosahexaenoic acid during
762 spermatogenesis. *J Biol Chem* **292**, 12065-12076,
763 doi:10.1074/jbc.M117.791277 (2017).
764 16 Shindou, H. *et al.* Docosahexaenoic acid preserves visual function by
765 maintaining correct disc morphology in retinal photoreceptor cells. *J Biol Chem*
766 **292**, 12054-12064, doi:10.1074/jbc.M117.790568 (2017).
767 17 Santiago, T. C., Zufferey, R., Mehra, R. S., Coleman, R. A. & Mamoun, C. B.
768 The Plasmodium falciparum PfGatp is an endoplasmic reticulum membrane
769 protein important for the initial step of malarial glycerolipid synthesis. *J Biol*
770 *Chem* **279**, 9222-9232, doi:10.1074/jbc.M310502200 (2004).
771 18 Lindner, S. E. *et al.* Enzymes involved in plastid-targeted phosphatidic acid
772 synthesis are essential for Plasmodium yoelii liver-stage development. *Mol*
773 *Microbiol* **91**, 679-693, doi:10.1111/mmi.12485 (2014).
774 19 Shears, M. J. *et al.* Characterization of the Plasmodium falciparum and P.
775 berghei glycerol 3-phosphate acyltransferase involved in FASII fatty acid
776 utilization in the malaria parasite apicoplast. *Cell Microbiol* **19**,
777 doi:10.1111/cmi.12633 (2017).
778 20 Vielemeyer, O., McIntosh, M. T., Joiner, K. A. & Coppens, I. Neutral lipid
779 synthesis and storage in the intraerythrocytic stages of Plasmodium falciparum.
780 *Mol Biochem Parasitol* **135**, 197-209, doi:10.1016/j.molbiopara.2003.08.017
781 (2004).
782 21 Palacpac, N. M. *et al.* Evidence that Plasmodium falciparum diacylglycerol
783 acyltransferase is essential for intraerythrocytic proliferation. *Biochem Biophys*
784 *Res Commun* **321**, 1062-1068, doi:10.1016/j.bbrc.2004.07.070 (2004).
785 22 Palacpac, N. M. *et al.* Developmental-stage-specific triacylglycerol biosynthesis,
786 degradation and trafficking as lipid bodies in Plasmodium falciparum-infected
787 erythrocytes. *J Cell Sci* **117**, 1469-1480, doi:10.1242/jcs.00988 (2004).
788 23 Nakanishi, H. *et al.* Cloning and characterization of mouse lung-type acyl-
789 CoA:lysophosphatidylcholine acyltransferase 1 (LPCAT1). Expression in
790 alveolar type II cells and possible involvement in surfactant production. *J Biol*
791 *Chem* **281**, 20140-20147, doi:10.1074/jbc.M600225200 (2006).

792 24 Zhukovsky, M. A., Filograna, A., Luini, A., Corda, D. & Valente, C. Phosphatidic
793 acid in membrane rearrangements. *FEBS Lett* **593**, 2428-2451,
794 doi:10.1002/1873-3468.13563 (2019).
795 25 Jarc, E. & Petan, T. Lipid Droplets and the Management of Cellular Stress. *Yale*
796 *J Biol Med* **92**, 435-452 (2019).
797 26 Aguado, B. & Campbell, R. D. Characterization of a human lysophosphatidic
798 acid acyltransferase that is encoded by a gene located in the class III region of
799 the human major histocompatibility complex. *J Biol Chem* **273**, 4096-4105,
800 doi:10.1074/jbc.273.7.4096 (1998).
801 27 Collins, C. R. *et al.* Robust inducible Cre recombinase activity in the human
802 malaria parasite Plasmodium falciparum enables efficient gene deletion within
803 a single asexual erythrocytic growth cycle. *Mol Microbiol* **88**, 687-701,
804 doi:10.1111/mmi.12206 (2013).
805 28 Tiburcio, M. *et al.* A Novel Tool for the Generation of Conditional Knockouts To
806 Study Gene Function across the Plasmodium falciparum Life Cycle. *mBio* **10**,
807 doi:10.1128/mBio.01170-19 (2019).
808 29 Birnbaum, J. *et al.* A genetic system to study Plasmodium falciparum protein
809 function. *Nat Methods* **14**, 450-456, doi:10.1038/nmeth.4223 (2017).
810 30 Zhang, M. *et al.* Uncovering the essential genes of the human malaria parasite
811 Plasmodium falciparum by saturation mutagenesis. *Science* **360**,
812 doi:10.1126/science.aap7847 (2018).
813 31 Lopez-Barragan, M. J. *et al.* Directional gene expression and antisense
814 transcripts in sexual and asexual stages of Plasmodium falciparum. *BMC*
815 *Genomics* **12**, 587, doi:10.1186/1471-2164-12-587 (2011).
816 32 Fagone, P. & Jackowski, S. Membrane phospholipid synthesis and
817 endoplasmic reticulum function. *J Lipid Res* **50 Suppl**, S311-316,
818 doi:10.1194/jlr.R800049-JLR200 (2009).
819 33 Wichers, J. S. *et al.* Dissecting the Gene Expression, Localization, Membrane
820 Topology, and Function of the Plasmodium falciparum STEVOR Protein Family.
821 *mBio* **10**, doi:10.1128/mBio.01500-19 (2019).
822 34 Yamamoto, Y. *et al.* Statistical distribution of single atoms and clusters of
823 supported Au catalyst analyzed by global high-resolution HAADF-STEM
824 observation with morphological image-processing operation. *Microscopy (Oxf)*
825 **63**, 209-218, doi:10.1093/jmicro/dfu001 (2014).
826 35 Imai, T. *et al.* Sub-nm 3D observation of human hair melanin by high-voltage
827 STEM. *Microscopy (Oxf)* **65**, 185-189, doi:10.1093/jmicro/dfv372 (2016).

828 36 Lazarus, M. D., Schneider, T. G. & Taraschi, T. F. A new model for hemoglobin
829 ingestion and transport by the human malaria parasite Plasmodium falciparum.
830 *J Cell Sci* **121**, 1937-1949, doi:10.1242/jcs.023150 (2008).
831 37 Slomianny, C. Three-dimensional reconstruction of the feeding process of the
832 malaria parasite. *Blood Cells* **16**, 369-378 (1990).
833 38 Yayon, A., Timberg, R., Friedman, S. & Ginsburg, H. Effects of chloroquine on
834 the feeding mechanism of the intraerythrocytic human malarial parasite
835 Plasmodium falciparum. *J Protozool* **31**, 367-372, doi:10.1111/j.1550-
836 7408.1984.tb02981.x (1984).
837 39 Abu Bakar, N., Klonis, N., Hanssen, E., Chan, C. & Tilley, L. Digestive-vacuole
838 genesis and endocytic processes in the early intraerythrocytic stages of
839 Plasmodium falciparum. *J Cell Sci* **123**, 441-450, doi:10.1242/jcs.061499
840 (2010).
841 40 Lawrence, C. & Olson, J. A. Birefringent hemozoin identifies malaria. *Am J Clin*
842 *Pathol* **86**, 360-363, doi:10.1093/ajcp/86.3.360 (1986).
843 41 Burda, P. C. *et al.* Global analysis of putative phospholipases in Plasmodium
844 falciparum reveals an essential role of the phosphoinositide-specific
845 phospholipase C in parasite maturation. *mBio* **14**, e0141323,
846 doi:10.1128/mbio.01413-23 (2023).
847 42 Flammersfeld, A., Lang, C., Flieger, A. & Pradel, G. Phospholipases during
848 membrane dynamics in malaria parasites. *Int J Med Microbiol* **308**, 129-141,
849 doi:10.1016/j.ijmm.2017.09.015 (2018).
850 43 Asad, M. *et al.* An essential vesicular-trafficking phospholipase mediates
851 neutral lipid synthesis and contributes to hemozoin formation in Plasmodium
852 falciparum. *BMC Biol* **19**, 159, doi:10.1186/s12915-021-01042-z (2021).
853 44 Bopp, S. *et al.* Potent acyl-CoA synthetase 10 inhibitors kill Plasmodium
854 falciparum by disrupting triglyceride formation. *Nat Commun* **14**, 1455,
855 doi:10.1038/s41467-023-36921-2 (2023).
856 45 Istvan, E. S. *et al.* Plasmodium Niemann-Pick type C1-related protein is a
857 druggable target required for parasite membrane homeostasis. *Elife* **8**,
858 doi:10.7554/eLife.40529 (2019).
859 46 Ramaprasad, A. *et al.* A malaria parasite phospholipase facilitates efficient
860 asexual blood stage egress. *PLoS Pathog* **19**, e1011449,
861 doi:10.1371/journal.ppat.1011449 (2023).
862 47 Henrici, R. C. *et al.* The Plasmodium falciparum Artemisinin Susceptibility-
863 Associated AP-2 Adaptin mu Subunit is Clathrin Independent and Essential for
864 Schizont Maturation. *mBio* **11**, doi:10.1128/mBio.02918-19 (2020).

865 48 Milani, K. J., Schneider, T. G. & Taraschi, T. F. Defining the morphology and
866 mechanism of the hemoglobin transport pathway in Plasmodium falciparum-
867 infected erythrocytes. *Eukaryot Cell* **14**, 415-426, doi:10.1128/EC.00267-14
868 (2015).
869 49 Sugiura, S. & Mima, J. Physiological lipid composition is vital for homotypic ER
870 membrane fusion mediated by the dynamin-related GTPase Sey1p. *Sci Rep* **6**,
871 20407, doi:10.1038/srep20407 (2016).
872 50 Bills, B. L. & Knowles, M. K. Phosphatidic Acid Accumulates at Areas of
873 Curvature in Tubulated Lipid Bilayers and Liposomes. *Biomolecules* **12**,
874 doi:10.3390/biom12111707 (2022).
875 51 Emoto, K. & Umeda, M. An essential role for a membrane lipid in cytokinesis.
876 Regulation of contractile ring disassembly by redistribution of
877 phosphatidylethanolamine. *J Cell Biol* **149**, 1215-1224,
878 doi:10.1083/jcb.149.6.1215 (2000).
879 52 Chen, Q. *et al.* Prefused lysosomes cluster on autophagosomes regulated by
880 VAMP8. *Cell Death Dis* **12**, 939, doi:10.1038/s41419-021-04243-0 (2021).
881 53 Furuta, N., Fujita, N., Noda, T., Yoshimori, T. & Amano, A. Combinational
882 soluble N-ethylmaleimide-sensitive factor attachment protein receptor proteins
883 VAMP8 and Vti1b mediate fusion of antimicrobial and canonical
884 autophagosomes with lysosomes. *Mol Biol Cell* **21**, 1001-1010,
885 doi:10.1091/mbc.e09-08-0693 (2010).
886 54 Nigg, E. A. Mitotic kinases as regulators of cell division and its checkpoints. *Nat*
887 *Rev Mol Cell Biol* **2**, 21-32, doi:10.1038/35048096 (2001).
888 55 Deshmukh, A. S. *et al.* Regulation of Plasmodium falciparum Origin Recognition
889 Complex subunit 1 (PfORC1) function through phosphorylation mediated by
890 CDK-like kinase PK5. *Mol Microbiol* **98**, 17-33, doi:10.1111/mmi.13099 (2015).
891 56 van Biljon, R. *et al.* Inducing controlled cell cycle arrest and re-entry during
892 asexual proliferation of Plasmodium falciparum malaria parasites. *Sci Rep* **8**,
893 16581, doi:10.1038/s41598-018-34964-w (2018).
894 57 Nozawa, A. *et al.* Characterization of mitochondrial carrier proteins of malaria
895 parasite Plasmodium falciparum based on in vitro translation and reconstitution.
896 *Parasitol Int* **79**, 102160, doi:10.1016/j.parint.2020.102160 (2020).
897 58 Tougan, T. *et al.* An automated haematology analyzer XN-30 distinguishes
898 developmental stages of falciparum malaria parasite cultured in vitro. *Malar J*
899 **17**, 59, doi:10.1186/s12936-018-2208-6 (2018).
900 59 Hayakawa, E. H. *et al.* Imaging of the subsurface structures of "unroofed"
901 Plasmodium falciparum-infected erythrocytes. *Exp Parasitol* **153**, 174-179,
902 doi:10.1016/j.exppara.2015.03.021 (2015).

903 60 Hayakawa, E. S. H. *et al.* Budding pouches and associated bubbles: 3D
904 visualization of exo-membrane structures in plasmodium falciparum
905 gametocytes. *Front Cell Infect Microbiol* **12**, 962495,
906 doi:10.3389/fcimb.2022.962495 (2022).
907 61 Kita, Y., Tokuoka, S. M., Oda, Y. & Shimizu, T. TRACES: A Lightweight
908 Browser for Liquid Chromatography-Multiple Reaction Monitoring-Mass
909 Spectrometry Chromatograms. *Metabolites* **12**, doi:10.3390/metabo12040354
910 (2022).

911

912 **Figure legends**

913 **Figure 1. A variety of microorganisms including *P. falciparum* have LPLATs with**

914 **partially conserved catalytic motifs.**

915 (A) Schematic diagram of phosphatidic acid (PA) synthesis from lysophosphatidic acid

916 (LPA). (B) Domain structure of PfLPLAT1. Transmembrane domain (TM) and AGPAT

917 domains (I to IV) were predicted using InterPro. (B) Multiple alignment of catalytic

918 motifs in LPLATs. Amino acid residues with ≥ 50% preservation across described

919 organisms are highlighted in yellow boxes. Acidic, basic, polar, and nonpolar amino

920 acids are shown as red, blue, green, and yellow letters, respectively, in the upper

921 sequence logo. (C) Predicted three-dimensional structures of PfLPLAT1 and

922 HsAGPAT1. Structural data were obtained from the AlphaFold Protein Structure

923 Database. Left panel: overviews. Right panel: magnified views around motifs I–IV.

924 Amino acid residues in motif I-IV are colored in magenta, green, cyan, and yellow.

925 More than 50% preserved residues are labeled.

926

927 **Figure 2. PfLPLAT1 shows LPAAT and LPCAT enzymatic activity.**

928 (A) Schematic image of LC-MS/MS based in vitro enzyme assay. Mixture of fatty acids

929 (acyl chain donors) are reacted with a deuterium-labeled LPLs in the presence of

930 PfLPLAT1 and diacyl forms of each lipid type with deuterium labeling were quantified.

931 (B, C) Recombinant PfLPLAT1 in proteo-liposomes generated from the wheat germ
932 expression system was detected by western blotting analysis (B) and Coomassie
933 Brilliant Blue (CBB) staining at the theoretical size (35 kDa). (D, E, F) PA (D), PC (E),
934 and PE (F) were estimated by LC-MS/MS-based analysis based on signal intensities
935 from standards (PA(34;1) for PA, PC(34:1) for PC, and PE(34:1) for PE estimation).
936 The x-axis shows product diacyl phospholipids with the sum of the carbons and double
937 bonds in two acyl chains (i.e., PA(34:1): total number of carbons in acyl chains = 34
938 and the number of double bonds = 1.
939
940 **Figure 3. PfLPLAT1 is essential in asexual replication and stage transition of *P.***
941 ***falciparum*.**
942 (A) Conditional gene knockout design for *Pflplat1* with the DiCre system. Arrows
943 indicate a transcription initiation site and the primer binding sites for PCR-based tests.
944 (B) Diagnostic PCR showed that the target gene was successfully replaced with the
945 targeting constructs: DNA segments were correctly amplified with f1/r1 (NF54::DiCre,
946 not amplified; *Pflplat1*:LoxPint:HA C9, 2676 bp), f2/r2 (NF54::DiCre, not amplified;
947 *Pflplat1*:LoxPint:HA C9, 979 bp), and f1/r2 (NF54::DiCre, 1027 bp; *Pflplat1*:LoxPint:HA
948 C9, not amplified) primer sets. (C–E) Conditional gene disruption of *Pflplat1* was
949 confirmed by PCR, western blotting, and immunofluorescence assay (IFA). (C) The

950 size of DNA amplicons for the 5' segment was shifted from 2676 to 784 bp at 24 hours
951 of rapamycin treatment. (D) Reductions in PfLPLAT1 were detected in
952 *Pflplat1*:LoxPint:HA clone C9 with anti-HA antibody at 24 and 48 hours of rapamycin
953 treatment. PfAldolase was used as an internal control for the total amount of proteins.
954 Theoretical molecular mass/kDa of HA-tagged PfLPLAT1 and PfAldolase is 37.4 and
955 40.0, respectively. Experiments were repeated three times. (E) Left panel:
956 representative immunofluorescence images of *Pflplat1*:LoxPint:HA C9 at 24 hours of
957 rapamycin treatment. Samples were stained for nuclei with DAPI (cyan) and PfLPLAT1
958 with anti-HA antibody (magenta) and analyzed by confocal microscopy. Scale bars: 2
959 μm. Right panel: violin plots showing the fluorescence intensity of HA-tagged
960 PfLPLAT1 in rapamycin-treated (+Rap) or untreated (−Rap) *Pflplat1*:LoxPint:HA C9 (n
961 = 20 per group). Violin plots range from the minimum to the maximum values. Dotted
962 bottom, middle, and top horizontal lines show 25th percentile, median, and 75th
963 percentile, respectively. Experiments were repeated two times. Statistical analysis
964 used F-test for equality of variance followed by two-tailed t-test. (F) Growth curve of
965 +Rap or −Rap *Pflplat1*:LoxPint:HA C9 and G6 clones. Data are shown as mean ± SD
966 from n = 3 independent biological replicates. (G) Overexpressed PfLPLAT1 rescued
967 parasite growth under the rapamycin treatment. Left panel: growth curve of +Rap or
968 −Rap *Pflplat1*:LoxPint:HA^{comp}. Data is shown as mean ± SD from n = 3 independent

969 biological replicates. Right panel: myc-tagged PfLPLAT1 expression in
970 *Pflplat1*:LoxPint:HA^{comp}. PfAldolase was used as an internal control for total amount of
971 protein. The theoretical molecular mass/kDa of myc-tagged PfLPLAT1 and PfAldolase
972 is 40.0. (H) Stage distributions of +Rap or −Rap *Pflplat1*:LoxPint:HA C9. Left panel:
973 representative images of Giemsa-stained blood films at described time points (4, 24,
974 30, 36, 44, and 48 hours post-infection [hpi]). Right: heatmap showing the parasite
975 stage distributions at the described time points. Data is shown as mean from n = 3
976 independent biological replicates.
977
978 **Figure 4. PfLPLAT1 colocalizes with endoplasmic reticulum throughout the all-**
979 **asexual stage.**
980 Left panel: representative confocal microscope images of parasites co-stained with
981 PfLPLAT1 and ER-resident protein BiP. Samples were stained for nuclei with DAPI
982 (blue), PfLPLAT1 with anti-HA antibody (green), and ER with anti-BiP antibody (red).
983 Scale bars = 2 μm. Right panel: signal profiles of anti-HA (green) and anti-BiP (red)
984 on white arrows in the overlays. Pearson's r values were calculated using overlays of
985 anti-HA and anti-BiP signal intensities to show the overlapping degree of both signals.
986

987 **Figure 5. *Pflplat1* deficiency led to the formation of abnormal cytostomes in**

988 **parasites.**

989 STEM images (bright-field) of −Rap (A, B) and +Rap (C-K) *Pflplat1*:LoxPint:HA at 36

990 hpi with 250 nm sections were obtained by a high-voltage transmission electron

991 microscope. (F) Magnified image of Figure 5E in a yellow dotted rectangle. (G, H)

992 Magnified images of Figure 5F in top (G) and bottom (H) yellow dotted rectangles.

993 Black arrowheads in (G) show vesicle-like structures and black arrows in (H) show the

994 parasite PPM and PVM. (J, K) Magnified images of Figure 5I in upper-left (J) and

995 bottom-right (H) yellow dotted rectangles. Black arrowhead in (J) shows a cytostome

996 with normal appearance. Scale bars = 2 μm (A–E), 500 nm (F, J, K), and 100 nm (G,

997 H). Small needle-like structures around the erythrocytes in Fig 5D and E are agar

998 particles, and they did not influence the internal structures of parasitized erythrocytes.

999

1000

1001 **Figure 6. *Pflplat1* deficiency influences the parasite transcriptomic profiles**

1002 **related to cell cycle progression.**

1003 (A) Volcano plot showing differentially expressed genes in +Rap versus −Rap

1004 *Pflplat1*:LoxPint:HA at 30 hpi (n = 3 independent biological replicates per group). Red

1005 dots are upregulated genes ($\log_2$FC > 0.5, adjusted p-value < 0.05) and blue dots are

1006 downregulated genes ($log_2FC < 0.5$, adjusted p-value < 0.05). Dotted vertical lines
1007 show 0.5 and −0.5 of log_2FC and dotted horizontal line shows 0.05 of adjusted p-value.
1008 Adjusted p-values were calculated using the Benjamini–Hochberg method. (B) Bar
1009 chart showing the number of downregulated genes classified into each biological
1010 process. P-values were calculated using the hypergeometric test. (C) Network
1011 diagram showing linkage of downregulated genes that are categorized in described
1012 biological processes. ACP, acyl carrier protein; ACS3, acyl-CoA synthetase 3; CAX,
1013 cation/H+ antiporter; CDF, cation diffusion facilitator; CNB, calcineurin subunit B;
1014 CRK4, cdc2-related protein kinase 4; CTR1, copper transporter 1; CuTP, copper-
1015 transporting ATPase; DGAT, diacylglycerol O-acyltransferase; DPCK, dephospho-
1016 CoA kinase; dUTPase, dUTP pyrophosphatase; DXR, 1-deoxy-D-xylulose 5-
1017 phosphate reductoisomerase; EST, exported serine/threonine protein kinase;
1018 FabB/FabF, 3-oxoacyl-acyl-carrier protein synthase I/II; FS, GDP-L-fucose synthase;
1019 GPI16, GPI transamidase component GPI16, putative; HCS1, biotin-protein ligase 1;
1020 ICMT, protein-S-isoprenylcysteine O-methyltransferase; IspD, 2-C-methyl-D-erythritol
1021 4-phosphate cytidylyltransferase; KDSR, 3-ketodihydrosphingosine reductase; MCM5,
1022 minichromosome maintenance complex component 5; Mei2, MEI2-like RNA-binding
1023 protein; MPC1, mitochondrial pyruvate carrier protein 1; MSH2-1, MutS protein
1024 homolog 2; MSH6, mutS homolog 6; NCAPD3, condensin-2 complex subunit D3; NDK,

1025 nucleoside diphosphate kinase; NEK3, NIMA-related kinase 3; NMT, peptide N-
1026 myristoyltransferase; ORC4, origin recognition complex subunit 4; OSCP, ATP
1027 synthase subunit O; PCMT1, protein-L-isoaspartate(D-aspartate) O-
1028 methyltransferase 1; PGM2, phosphoglucomutase-2; PIGA, phosphatidylinositol N-
1029 acetylglucosaminyltransferase subunit A; PIGL, N-acetylglucosaminyl-
1030 phosphatidylinositol de-N-acetylase; PK5, protein kinase 5; PMT,
1031 phosphoethanolamine N-methyltransferase; PPKL, protein phosphatase-containing
1032 kelch-like domains; PPRD, polyprenol reductase; PREX, plastid replication-repair
1033 enzyme; PPT, phosphoenolpyruvate/phosphate translocator; RCC, regulator of
1034 chromosome condensation; RRM1, ribonucleotide reductase catalytic subunit M1;
1035 SAS6, spindle assembly abnormal protein 6; SCD, stearoyl-CoA desaturase; SR12,
1036 serpentine receptor 12; SRD5A, 3-oxo-5-alpha-steroid 4-dehydrogenase; SRPK,
1037 serine/threonine protein kinase; TERT, telomerase reverse transcriptase; TOP3, DNA
1038 topoisomerase 3; UBA3, ubiquitin like modifier activating enzyme 3; UDG, uracil-DNA
1039 glycosylase; UGT, UDP-galactose transporter; ZIPCO, ZIP domain-containing protein.
1040

1041 **Figure 7. *Pflplat1* deficiency induced modified phospholipid profiles in parasites.**
1042 (A–D) Bar graphs showing area values of PA (A), PE (B), PC (C), and SM species (D)
1043 in +Rap and −Rap *Pflplat1*:LoxPint:HA at 30 hpi. Extracted lipids from an equal

1044 number of parasites were analyzed by LC-MS/MS. (E) Dot plots showing the total area

1045 values of PA (excluding LPA signals), PE, PC (excluding LPC signals), and SM in

1046 −Rap and +Rap *Pflplat1*:LoxPint:HA at 30 hpi. Data are shown as mean ± SD from n

1047 = 3 independent biological replicates. P-values were calculated using unpaired two-

1048 tailed t-test (*, $P < 0.05$; **, $P < 0.01$, ***, $P < 0.005$).

1049

1050 **Figure 8. Schematic diagram showing the effect of *Pflplat1* deletion on parasites.**

1051 **Supplementary materials**

1052 **Figure S1. Plasmid DNA integration and *Pf*lplat1-knockout efficiency in**

1053 ***Pflplat1*:LoxPint:HA G6 clonal line.**

1054 (A) Diagnostic PCR was performed to check whether the construct was correctly

1055 integrated into the target locus. DNA segments were amplified with f1/r1 (NF54::DiCre,

1056 not amplified; *Pflplat1*:LoxPint:HA G6, 2676 bp), f2/r2 (NF54::DiCre, not amplified;

1057 *Pflplat1*:LoxPint:HA G6, 979 bp), and f1/r2 (NF54::DiCre, 1027 bp; *Pflplat1*:LoxPint:HA

1058 G6, not amplified) primer sets. (B–D) Conditional knockout of *Pflplat1* was confirmed

1059 by PCR, western blotting, and IFA. (B) The size of DNA amplicons was shifted from

1060 2676 to 784 bp at 24 hours of rapamycin treatment. (C) A reduction in PfLPLAT1

1061 expression was detected in *Pflplat1*:LoxPint:HA G6 with anti-HA antibody at 24 and

1062 48 hours of rapamycin treatment. PfAldolase was used as an internal control.

1063 Experiments were repeated three times. (D) Left panel: representative

1064 immunofluorescence micrographs of *Pflplat1*:LoxPint:HA G6 at 24 hours of rapamycin

1065 treatment. Samples were stained for nuclei with DAPI (cyan) and PfLPLAT1 with anti-

1066 HA antibody (magenta) and scanned using confocal microscopy. Scale bars = 2 μm.

1067 Right panel: violin plots showing the fluorescence intensity of HA-tagged PfLPLAT1 in

1068 rapamycin-treated (+Rap) or untreated (−Rap) *Pflplat1*:LoxPint:HA G6 (n = 20 per

1069 group). Violin plots range from minimum to maximum values. Dotted bottom, middle,

1070 and top horizontal lines show 25th percentile, median, and 75th percentile.
1071 Experiments were repeated two times. Statistical analysis was performed using F-test
1072 for equality of variance followed by two-tailed t-test.
1073
1074 **Figure S2. *Pflplat1* deletion did not influence gametocyte maturation.**
1075 (A) Conditional knockout of *Pflplat1* in gametocytes was checked by performing PCR
1076 at day 14 after gametocytogenesis. The size of DNA amplicons was shifted from 2676
1077 to 784 bp. (B) Gametocytemia of +Rap or −Rap *Pflplat1*:LoxPint:HA on days 12–15
1078 after gametocytogenesis. Data are shown as mean ± SD from n = 3 independent
1079 biological replicates. (C) Heatmap showing gametocyte stage distribution of +Rap and
1080 −Rap *Pflplat1*:LoxPint:HA. Data are shown as mean from n = 3 independent biological
1081 replicates.
1082
1083 **Figure S3. *Pflplat1* deletion reduces the size of hemozoin in parasites.**
1084 Left panel: violin plots showing the size of hemozoin in +Rap or −Rap
1085 *Pflplat1*:LoxPint:HA (n = 60 per group). Violin plots range from minimum to maximum
1086 values. Dotted bottom, middle, and top horizontal lines show 25th percentile, median,
1087 and 75th percentile. Data was combined from three independent experiments (n = 20

1088 per group per experiment). Statistical analysis was performed using the Wilcoxon
1089 signed-rank test.
1090 Right panel: representative polarized light micrographs of *Pflplat1*:LoxPint:HA at 30
1091 hpi. Images were obtained with “crossed polars” and a 100× HCX PL FLUOTAR
1092 objective (n = 1.32)-equipped Leica DMi8 fluorescence microscope. Scale bars = 2
1093 μm.
1094
1095 **Figure S4. Transcriptomic analysis of transgenic parasites at 24 and 30 hpi.**
1096 (A) Volcano plot showing DEGs in +Rap versus −Rap *Pflplat1*:LoxPint:HA at 24 hpi (n
1097 = 3 independent biological replicates per group). Blue dots indicate downregulated
1098 genes ($\log_2$FC < 0.5, adjusted p-value < 0.05). Dotted vertical lines show 0.5 and −0.5
1099 of $\log_2$FC and dotted horizontal line shows 0.05 of the adjusted p-value. Adjusted p-
1100 values were calculated using the Benjamini–Hochberg method. (B) Principal
1101 component analysis of gene expression profiles in +Rap and −Rap samples at 24 and
1102 30 hpi. (C) Heatmaps showing the Pearson correlation coefficient between gene
1103 expression profiles in +Rap and −Rap *Pflplat1*:LoxPint:HA at 24 and 30 hpi.
1104
1105 **Figure S5. *Pflplat1* deficiency affects the profile of phospholipids in parasites.**

1106 (A–D) Bar graphs showing normalized fractions of PA (A), PE (B), PC (C), and SM (D)

1107 against the total area values within the same type of lipid in +Rap and −Rap

1108 *Pflplat1*:LoxPint:HA at 30 hpi. Data are shown as mean ± SD from n = 3 independent

1109 biological replicates. P-values were calculated using unpaired two-tailed t-test (*, $P <$

1110 0.05; **, $P < 0.01$, ***, $P < 0.005$).

1111

1112 **Table S1. Primers used in this study**

1113 **Table S2. DEG list and GO analysis results**

Figure 1

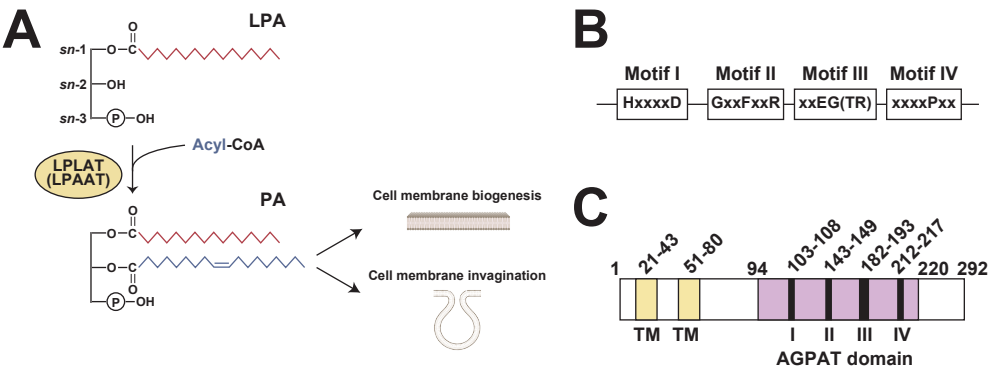

D

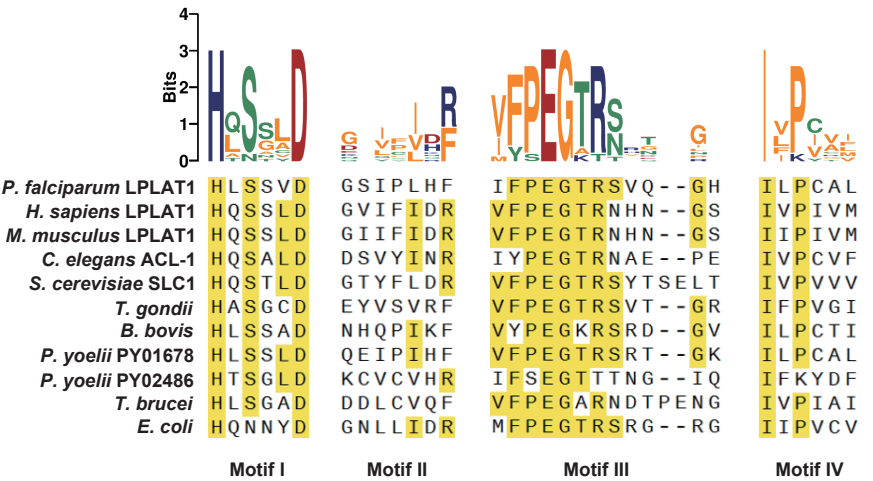

E

P. falciparum LPLAT1

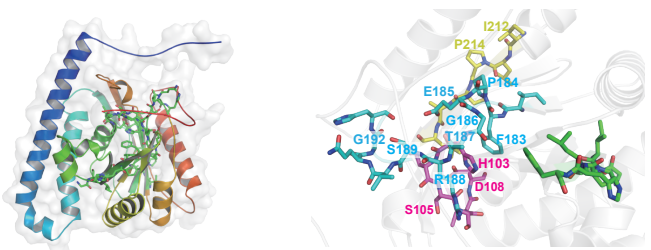

H. sapiens LPLAT1

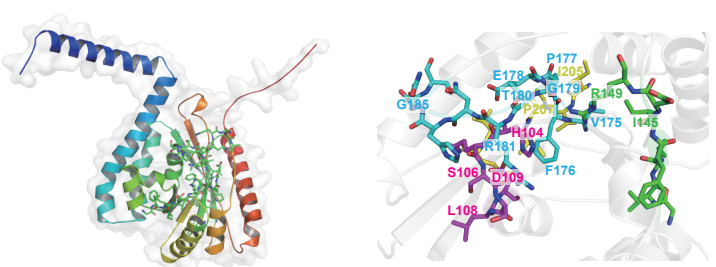

Figure 2

A

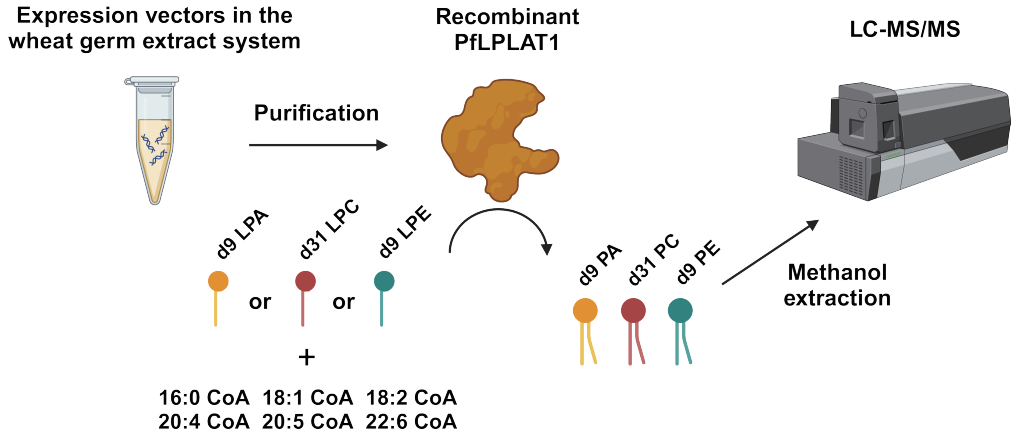

B

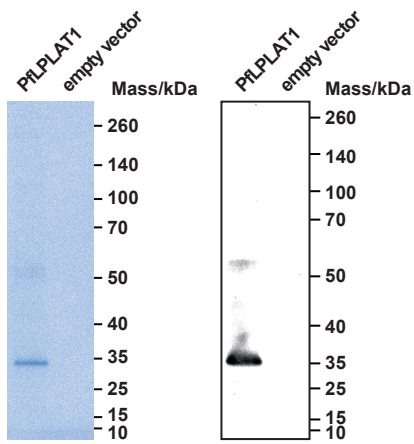

C

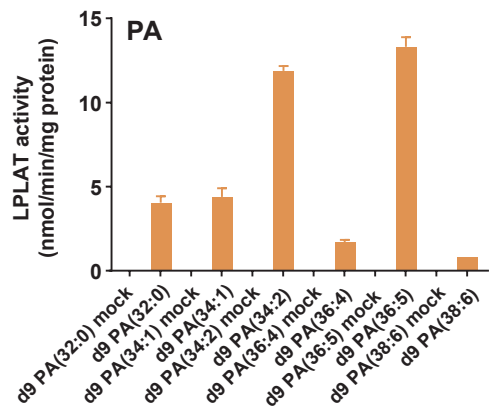

D

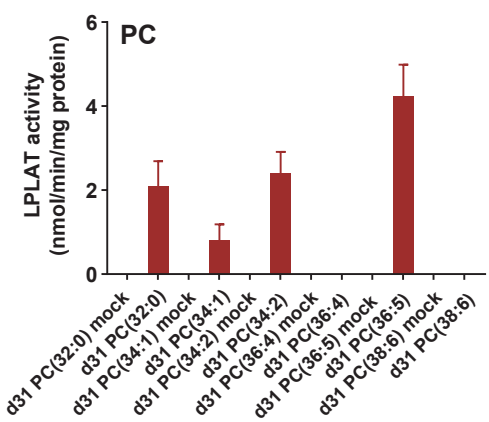

E

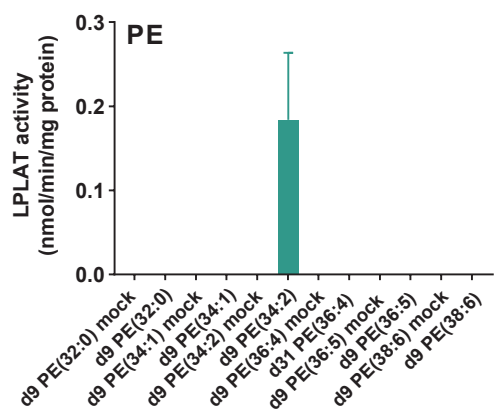

Figure 3

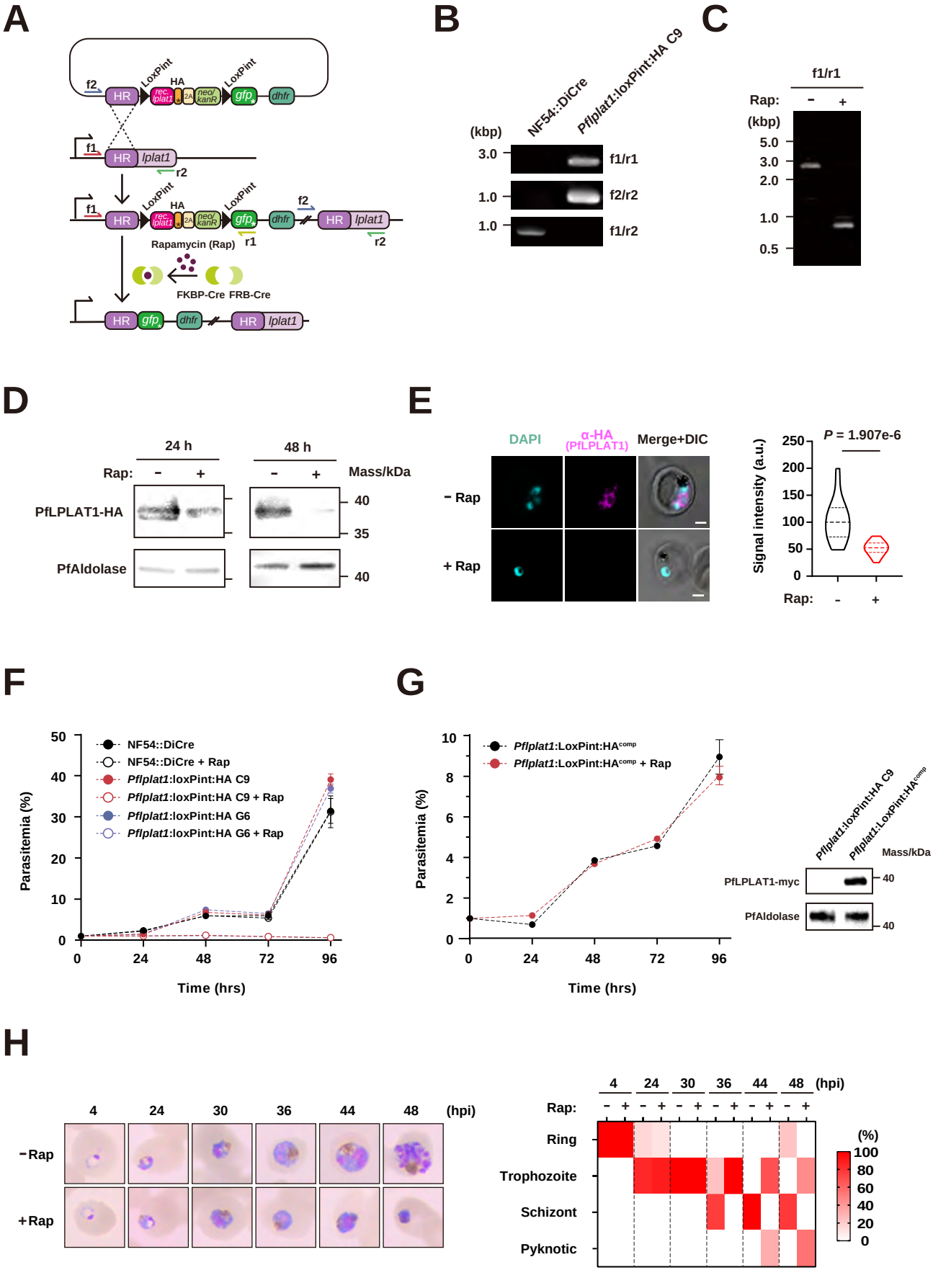

A
f2
HR
LoxPint
HA
rec. lplat1
2A
neo/ kanR
LoxPint
gfp
dhfr
f1
HR
lplat1
r2
f1
HR
LoxPint
HA
rec. lplat1
2A
neo/ kanR
LoxPint
gfp
dhfr
f2
HR
lplat1
r1
r2
Rapamycin (Rap)
FKBP-Cre
FRB-Cre
HR
gfp
dhfr
HR
lplat1
B
NF54::DiCre
Pflplat1:loxPint:HA C9
(kbp)
3.0
1.0
1.0
f1/r1
f2/r2
f1/r2
C
f1/r1
Rap:
-
+
(kbp)
5.0
3.0
2.0
1.0
0.5
D
24 h
48 h
Rap:
-
+
-
+
Mass/kDa
PfLPLAT1-HA
PfAldolase
40
35
40
E
DAPI
α-HA (PfLPLAT1)
Merge+DIC
- Rap
+ Rap
P = 1.907e-6
Signal intensity (a.u.)
250
200
150
100
50
0
Rap:
-
+
F
NF54::DiCre
NF54::DiCre + Rap
Pflplat1:loxPint:HA C9
Pflplat1:loxPint:HA C9 + Rap
Pflplat1:loxPint:HA G6
Pflplat1:loxPint:HA G6 + Rap
Parasitemia (%)
50
40
30
20
10
0
0
24
48
72
96
Time (hrs)
G
Pflplat1:LoxPint:HAcomp
Pflplat1:LoxPint:HAcomp + Rap
Parasitemia (%)
10
8
6
4
2
0
0
24
48
72
96
Time (hrs)
Pflplat1:loxPint:HA C9
Pflplat1:LoxPint:HAcomp
Mass/kDa
PfLPLAT1-myc
PfAldolase
40
40
H
4
24
30
36
44
48
(hpi)
-Rap
+Rap
4
24
30
36
44
48
(hpi)
Rap:
- + - + - + - + - + - +
Ring
Trophozoite
Schizont
Pyknotic
(%)
100
80
60
40
20
0

Figure 4

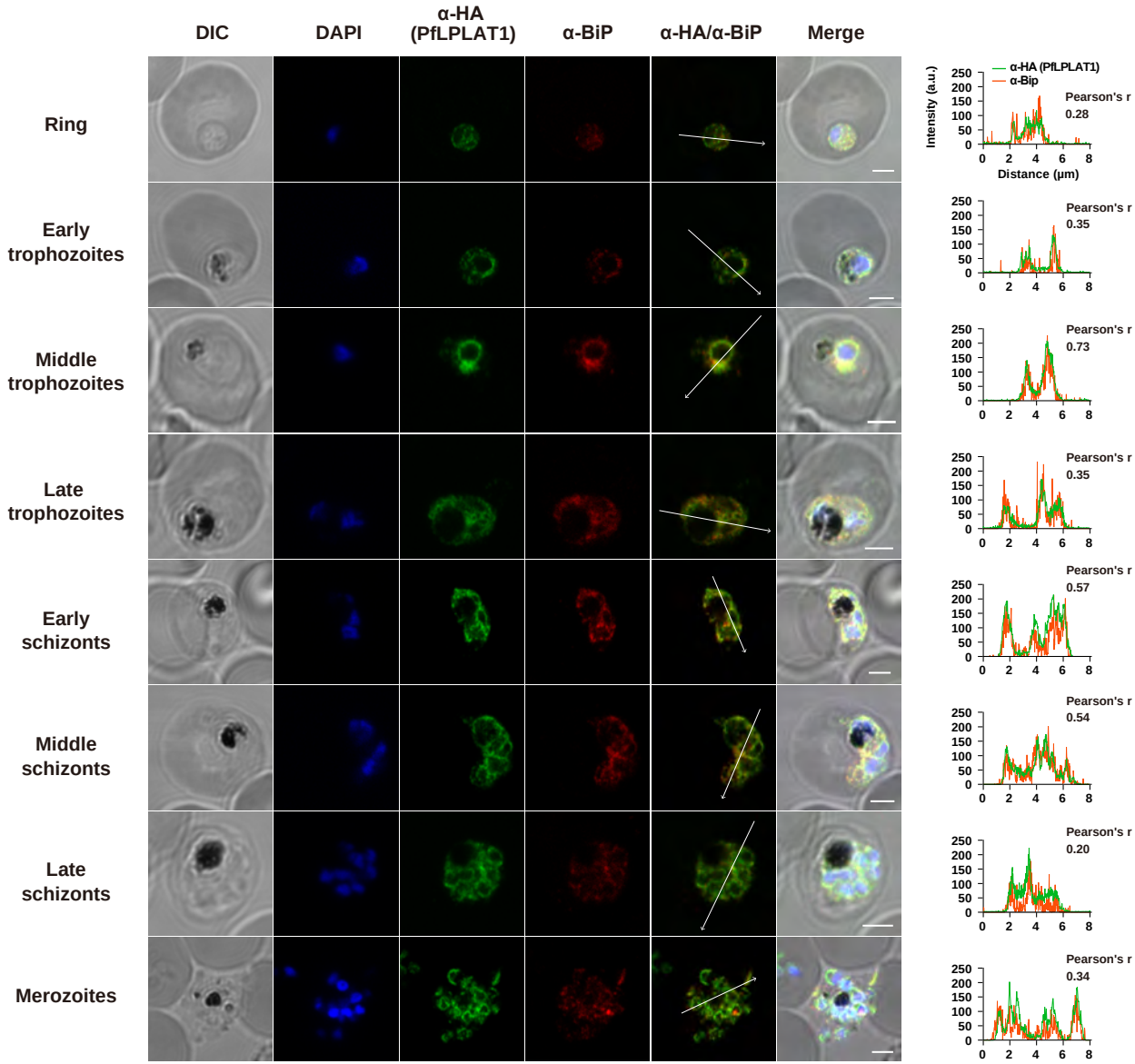
DIC
DAPI
α-HA (PfLPLAT1)
α-BiP
α-HA/α-BiP
Merge
Ring
Early trophozoites
Middle trophozoites
Late trophozoites
Early schizonts
Middle schizonts
Late schizonts
Merozoites
α-HA (PfLPLAT1)
α-Bip
Intensity (a.u.)
Distance (μm)
Pearson's r
0.28
0.35
0.73
0.35
0.57
0.54
0.20
0.34

Figure 5

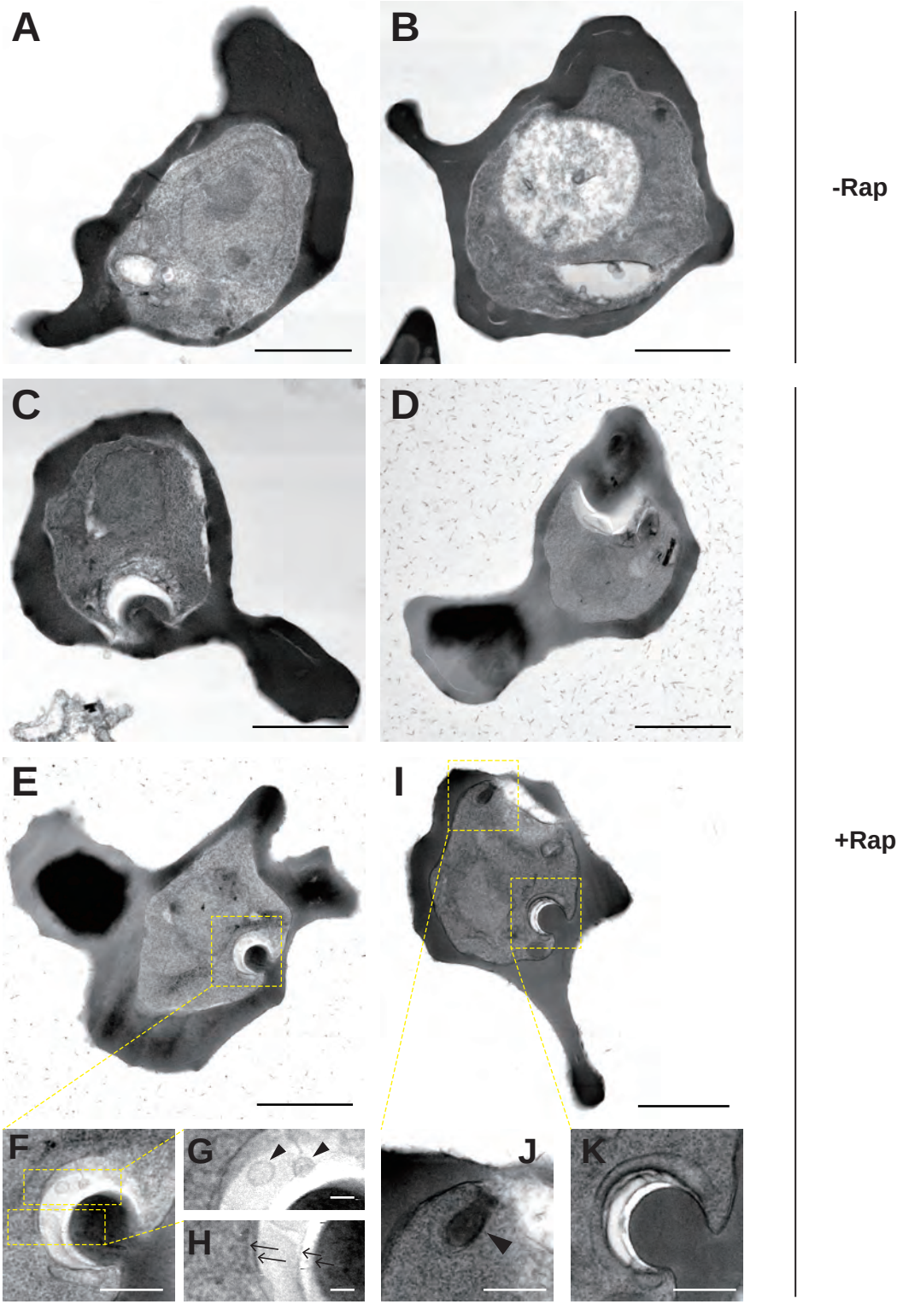

Figure 6

A

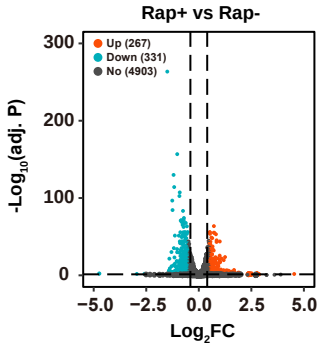
Rap+ vs Rap-
Up (267)
Down (331)
No (4903)
-Log10(adj. P)
300
200
100
0
−5.0
−2.5
0.0
2.5
5.0
Log2FC

B

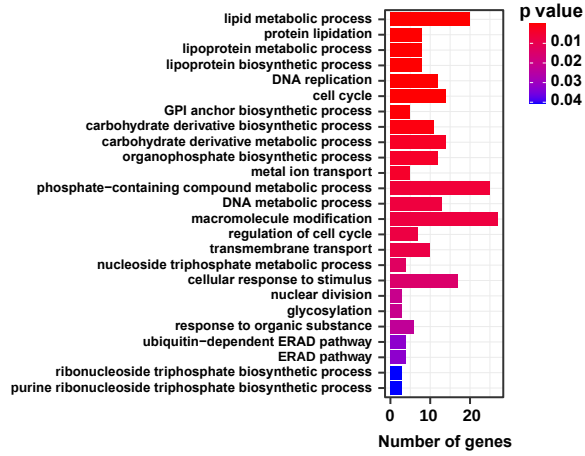
lipid metabolic process
protein lipidation
lipoprotein metabolic process
lipoprotein biosynthetic process
DNA replication
cell cycle
GPI anchor biosynthetic process
carbohydrate derivative biosynthetic process
carbohydrate derivative metabolic process
organophosphate biosynthetic process
metal ion transport
phosphate−containing compound metabolic process
DNA metabolic process
macromolecule modification
regulation of cell cycle
transmembrane transport
nucleoside triphosphate metabolic process
cellular response to stimulus
nuclear division
glycosylation
response to organic substance
ubiquitin−dependent ERAD pathway
ERAD pathway
ribonucleoside triphosphate biosynthetic process
purine ribonucleoside triphosphate biosynthetic process
p value
0.01
0.02
0.03
0.04
0
10
20
Number of genes

C

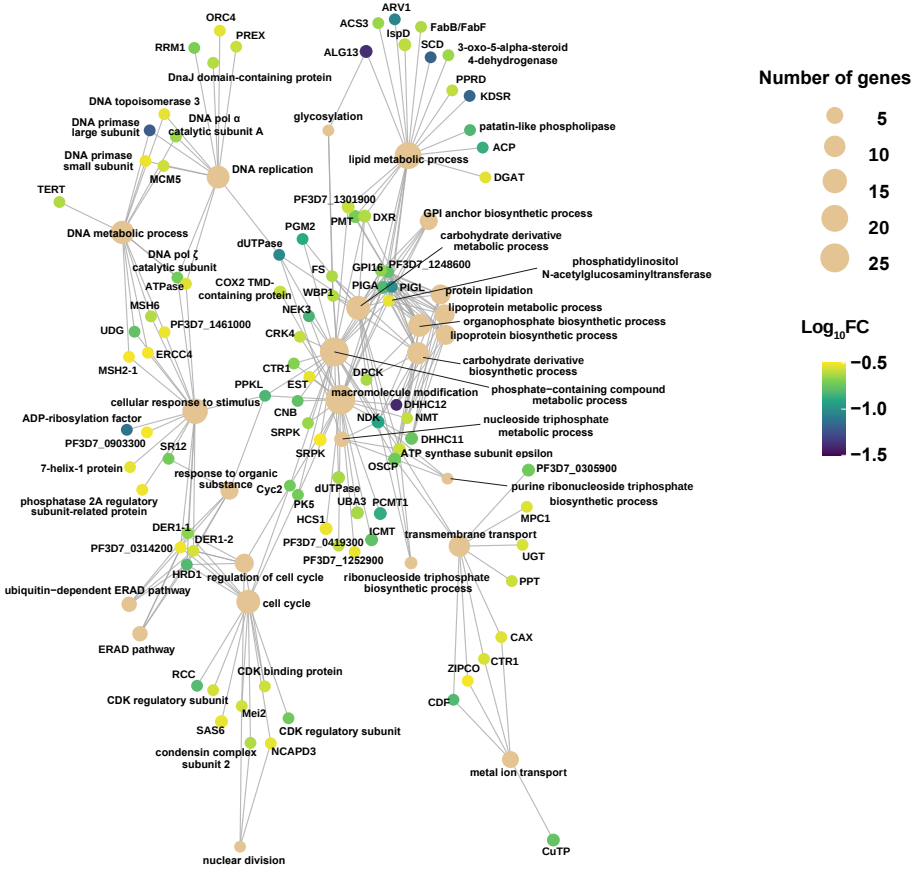
ORC4
PREX
RRM1
DnaJ domain-containing protein
DNA topoisomerase 3
DNA primase large subunit
DNA pol α catalytic subunit A
DNA primase small subunit
MCM5
DNA replication
TERT
DNA metabolic process
DNA pol ζ catalytic subunit
ATPase
COX2 TMD-containing protein
MSH6
PF3D7_1461000
UDG
ERCC4
MSH2-1
ADP-ribosylation factor
PF3D7_0903300
SR12
7-helix-1 protein
cellular response to stimulus
response to organic substance
phosphatase 2A regulatory subunit-related protein
DER1-1
DER1-2
PF3D7_0314200
HRD1
ubiquitin−dependent ERAD pathway
regulation of cell cycle
cell cycle
ERAD pathway
RCC
CDK binding protein
CDK regulatory subunit
Mei2
SAS6
CDK regulatory subunit
condensin complex subunit 2
NCAPD3
nuclear division
ARV1
ACS3
FabB/FabF
IspD
ALG13
SCD
3-oxo-5-alpha-steroid 4-dehydrogenase
PPRD
KDSR
glycosylation
patatin-like phospholipase
ACP
lipid metabolic process
DGAT
PF3D7_1301900
PMT
DXR
GPI anchor biosynthetic process
PGM2
dUTPase
carbohydrate derivative metabolic process
FS
GPI16
PF3D7_1248600
phosphatidylinositol N-acetylglucosaminyltransferase
WBP1
PIGA
PIGL
protein lipidation
NEK3
lipoprotein metabolic process
organophosphate biosynthetic process
CRK4
lipoprotein biosynthetic process
carbohydrate derivative biosynthetic process
CTR1
DPCK
EST
PPKL
macromolecule modification
phosphate−containing compound metabolic process
DHHC12
CNB
NDK
NMT
nucleoside triphosphate metabolic process
SRPK
DHHC11
ATP synthase subunit epsilon
OSCP
PF3D7_0305900
purine ribonucleoside triphosphate biosynthetic process
Cyc2
dUTPase
PK5
UBA3
PCMT1
HCS1
MPC1
ICMT
transmembrane transport
PF3D7_0419300
PF3D7_1252900
UGT
ribonucleoside triphosphate biosynthetic process
PPT
CAX
CTR1
ZIPCO
CDF
metal ion transport
CuTP
Number of genes
5
10
15
20
25
Log10FC
−0.5
−1.0
−1.5

Figure 7

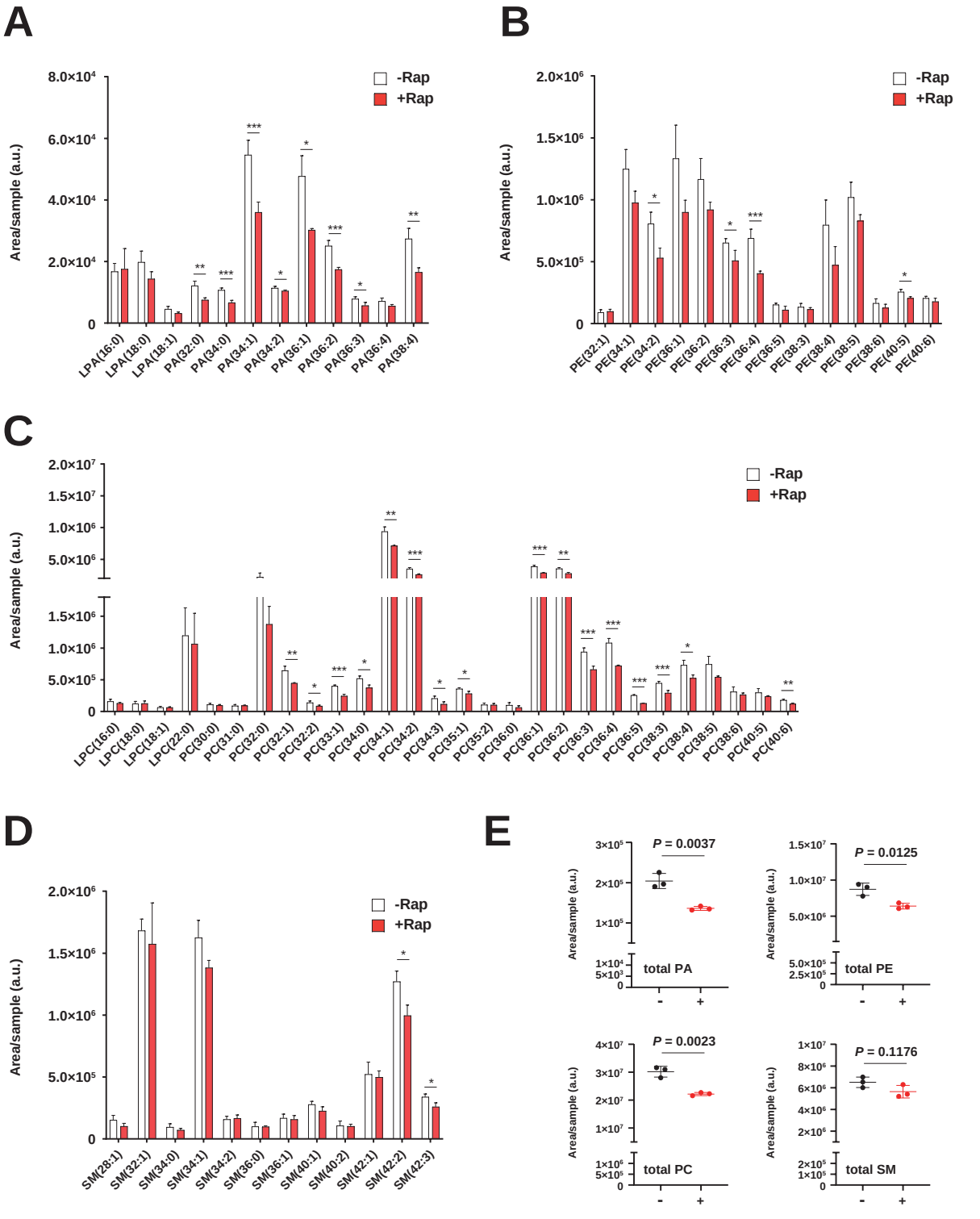
A
B
C
D
E
-Rap
+Rap
Area/sample (a.u.)
LPA(16:0)
LPA(18:0)
LPA(18:1)
PA(32:0)
PA(34:0)
PA(34:1)
PA(34:2)
PA(36:1)
PA(36:2)
PA(36:3)
PA(36:4)
PA(38:4)
PE(32:1)
PE(34:1)
PE(34:2)
PE(36:1)
PE(36:2)
PE(36:3)
PE(36:4)
PE(36:5)
PE(38:3)
PE(38:4)
PE(38:5)
PE(38:6)
PE(40:5)
PE(40:6)
LPC(16:0)
LPC(18:0)
LPC(18:1)
LPC(22:0)
PC(30:0)
PC(31:0)
PC(32:0)
PC(32:1)
PC(32:2)
PC(33:1)
PC(34:0)
PC(34:1)
PC(34:2)
PC(34:3)
PC(35:1)
PC(35:2)
PC(36:0)
PC(36:1)
PC(36:2)
PC(36:3)
PC(36:4)
PC(36:5)
PC(38:3)
PC(38:4)
PC(38:5)
PC(38:6)
PC(40:5)
PC(40:6)
SM(28:1)
SM(32:1)
SM(34:0)
SM(34:1)
SM(34:2)
SM(36:0)
SM(36:1)
SM(40:1)
SM(40:2)
SM(42:1)
SM(42:2)
SM(42:3)
P = 0.0037
total PA
P = 0.0125
total PE
P = 0.0023
total PC
P = 0.1176
total SM

Figure 8

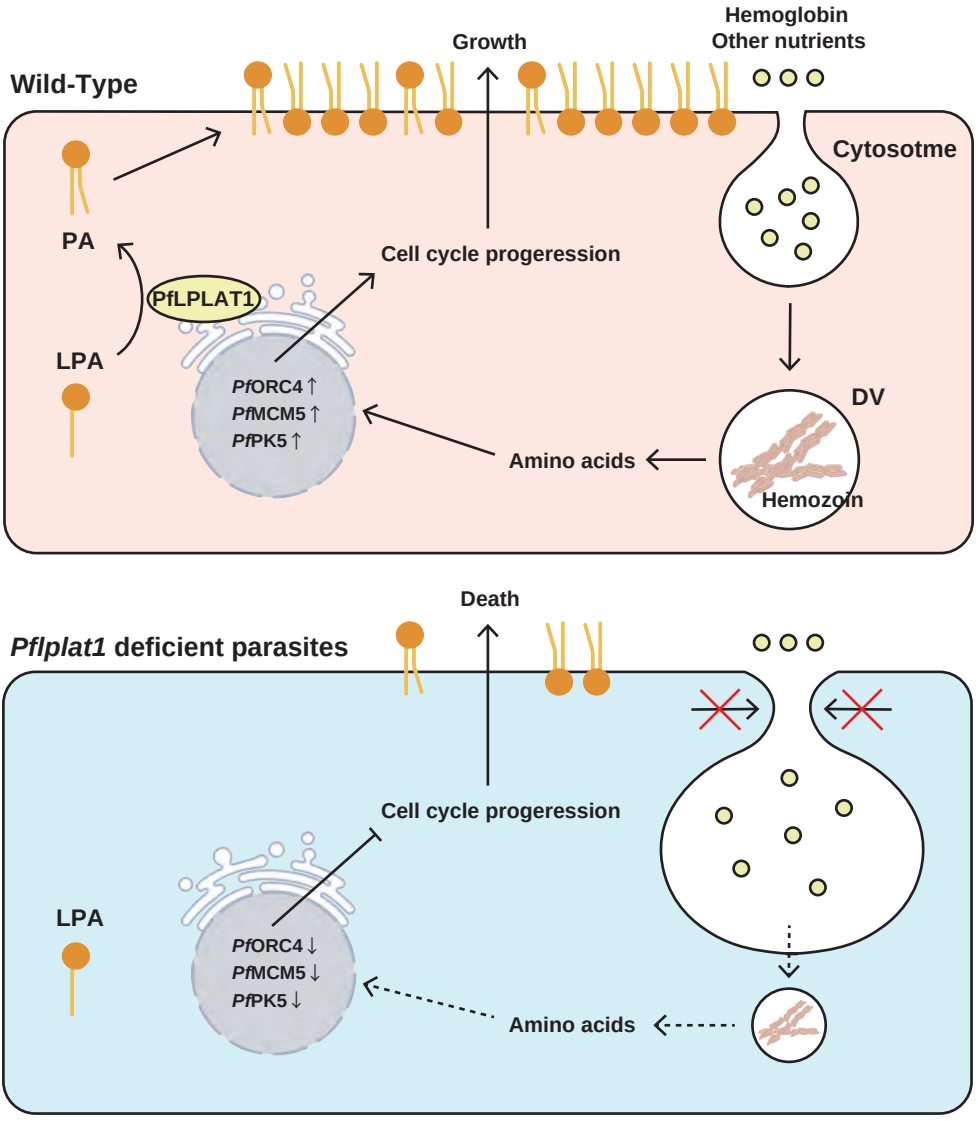
Wild-Type
Growth
Hemoglobin
Other nutrients
Cytosotme
PA
Cell cycle progeression
PfLPLAT1
LPA
PfORC4↑
PfMCM5↑
PfPK5↑
DV
Amino acids
Hemozoin
Death
Pflplat1 deficient parasites
Cell cycle progeression
LPA
PfORC4↓
PfMCM5↓
PfPK5↓
Amino acids

Table 1. Currently known human LPLATs.

Family	Proposed Name	NCBI information			
		Current Official Symbol	Organism	Reference Sequence	Gene ID
AGPAT	LPLAT1	AGPAT1	human	NM_032741	10554
	LPLAT2	AGPAT2	human	NM_006412	10555
	LPLAT3	AGPAT3	human	NM_001037553	56894
	LPLAT4	AGPAT4	human	NM_020133	56895
	LPLAT5	AGPAT5	human	NM_018361	55326
	LPLAT6	LCLAT1	human	NM_182551	253558
	LPLAT7	LPGAT1	human	NM_014873	9926
	LPLAT8	LPCAT1	human	NM_024830	79888
	LPLAT9	LPCAT2	human	NM_017839	54947
	LPLAT10	LPCAT4	human	NM_153613	254531
MBOAT	LPLAT11	MBOAT7	human	NM_024298	79143
	LPLAT12	LPCAT3	human	NM_005768	10162
	LPLAT13	MBOAT2	human	NM_138799	129642
	LPLAT14	MBOAT1	human	NM_001080480	154141

LCLAT: Lysocardiolipin Acyltransferase